



HAL
open science

tLyp-1: A peptide suitable to target NRP-1 receptor

Ludivine Larue, Bibigul Kenzhebayeva, Mohammad Al-Thiabat, Valérie Jouan-Hureaux, Amirah Mohd Gazzali, Habibah Wahab, Cédric Boura, Gulzhakhan Yeligbayeva, Ulantay Nakan, Céline Frochot, et al.

► To cite this version:

Ludivine Larue, Bibigul Kenzhebayeva, Mohammad Al-Thiabat, Valérie Jouan-Hureaux, Amirah Mohd Gazzali, et al. tLyp-1: A peptide suitable to target NRP-1 receptor. *Bioorganic Chemistry*, 2023, 130, pp.106200. 10.1016/j.bioorg.2022.106200 . hal-03863449

HAL Id: hal-03863449

<https://hal.univ-lorraine.fr/hal-03863449v1>

Submitted on 28 Nov 2022

HAL is a multi-disciplinary open access archive for the deposit and dissemination of scientific research documents, whether they are published or not. The documents may come from teaching and research institutions in France or abroad, or from public or private research centers.

L'archive ouverte pluridisciplinaire **HAL**, est destinée au dépôt et à la diffusion de documents scientifiques de niveau recherche, publiés ou non, émanant des établissements d'enseignement et de recherche français ou étrangers, des laboratoires publics ou privés.



Distributed under a Creative Commons Attribution - NonCommercial - NoDerivatives 4.0 International License

tLyp-1: a peptide suitable to target NRP-1 receptor

Ludivine Larue^{a,b,†}, Bibigul Kenzhebayeva^{a,c,†}, Mohammad G. Al-Thiabat^d, Valérie Jouan-Hureau^c, Amirah Mohd-Gazzali^d, Habibah A. Wahab^d, Cédric Boura^c, Gulzhakhan Yeligbayeva^c, Ulantay Nakan^c, Céline Frochot^b, Samir Acherar^{a,*}

^a Université de Lorraine, CNRS, LCPM, F-54000 Nancy, France;

^b Université de Lorraine, CNRS, LRGP, F-54000 Nancy, France;

^c Institute of Geology and Oil-gas Business, Satbayev University, Almaty 050013, Kazakhstan;

^d School of Pharmaceutical Sciences, Universiti Sains Malaysia, 11800 Penang, Malaysia;

* Corresponding author: samir.acherar@univ-lorraine.fr, +33 3 72 74 36 87

† These authors contributed equally to this work.

Abstract:

Targeting vascular endothelial growth factor receptor (VEGFR) and its co-receptor neuropilin-1 (NRP-1) is an interesting vascular strategy. tLyp-1 is a tumor-homing and penetrating peptide of 7 amino acids (CGNKRTR). It is a truncated form of Lyp-1 (CGNKRTRGC), which is known to target NRP-1 receptor, with high affinity and specificity. It is mediated by endocytosis *via* C-end rule (CendR) internalization pathway. The aim of this study is to evaluate the importance of each amino acid in the tLyp-1 sequence through alanine-scanning (Ala-scan) technique, during which each of the amino acid in the sequence was systematically replaced by alanine to produce 7 different analogues. *In silico* approach through molecular docking and molecular dynamics are employed to understand the interaction between the peptide and its analogues with the NRP-1 receptor, followed by *in vitro* ligand binding assay study. The C-terminal Arg is crucial in the interaction of tLyp-1 with NRP-1 receptor. Substituting this residue dramatically reduces the affinity of this peptide which is clearly seen in this study. Lys-4 is also important in the interaction, which is confirmed *via* the *in vitro* study and the MM-PBSA analysis. The finding in this study supports the CendR, in which the presence of R/K-XX-R/K motif is essential in the binding of a ligand with NRP-1 receptor. This presented work will serve as a guide in the future work pertaining the development of active targeting agent towards NRP-1 receptor.

Keywords: tLyp-1 peptide; NRP-1; Targeting; Alanine-scanning; Molecular docking; Molecular dynamic; Radius of gyration (Rg); H-bonds; MM-PBSA per residue energy decomposition; *In vitro* ligand binding

List of abbreviations:

ADMET: Absorption, Distribution, Metabolism, Excretion, and Toxicity; Boc, tert-ButOxyCarbonyl; tBu, Tert-butyl; BSA, Bovine Serum Albumin; DMF, DiMethylFormamide; DMSO, DiMethylSulfOxide; FEB, Free Energy of Binding; Fmoc, Fluorenylmethoxycarbonyl; HBTU, 2-(1H-Benzotriazol-1-yl)-1,1,3,3-TetramethylUronium hexafluorophosphate; HPLC, High Performance Liquid Chromatography; HRMS, High Resolution Mass Spectrometry; LBA, Ligand Binding Assay; NMM, N-MethylMorpholine; NMP, N-MethylPyrrolidine; NRP-1, Neuropilin-1; Pbf, Pentamethyl-2,3-dihydrobenzofuran-5-sulfonyl; PBS, Phosphate Buffer Saline; PDB, Protein Data Bank; PDT, Photodynamic Therapy; PS, Photosensitizer; RMSD, Root-Mean-Square Deviation; TFA, TriFluoroacetic Acid; TIPS, TriIsoPropylSilane; Trt, Triphenylmethyl; VEGF, Vascular Endothelial Growth Factor; VEGFR, Vascular Endothelial Growth Factor Receptor.

1. Introduction

Thanks to the development of new therapies or drugs, a decline of incidence and death rates can be observed for all cancers.¹ Nevertheless, there are still a lot of room for improvement and progress that still need to be done. Improvement of drug selectivity could offer better treatment efficacy with potentially lower doses. One strategy consists of targeting neo-blood vessels to induce an asphyxia of the tumor by preventing the supply of oxygen and nutrient from reaching the tumor cells.

The application of peptides in targeted drug delivery are being widely explored and numerous peptides were reported to have the potential as active targeting agents. Peptides refer to molecules with a specific sequence of less than 50 amino acids. They are useful to improve the delivery of payloads, such as bonded drugs to targeted cells, while reducing unwanted side effects of drugs to healthy tissues.² Several commonly described peptides include the tumor homing peptides such as the RGD sequence and its cyclic derivatives (cRGD) that target the integrin $\alpha\beta3$ which are overly expressed in endothelial cells.

Since many years, our team has focus on the development of targeted photosensitizers (PSs) for photodynamic therapy (PDT) applications. In particular, we have designed PSs coupled to peptides targeting neuropilin-1 (NRP-1) receptor, which is a co-receptor of vascular endothelial growth factor receptor (VEGFR) that is overexpressed on tumors and neo-vessels. Beginning with ATWLPPR^{3,4} as the targeting peptide that was subsequently proved to be not so stable *in vivo*, we continue to develop several other peptides such as KDKPPR.⁵⁻⁹ In this new study, we explored tLyp-1, a tumor-homing and penetrating peptide that consists of 7 amino acids (CGNKRTR). It is a truncated form of Lyp-1 (CGNKRTRGC), a cyclic 9-amino acid peptide, which is known to target tumor lymphatics as well as tumor cells and associated macrophages especially.^{10,11} It is mediated by endocytosis *via* the C-end rule (CendR) internalization pathway.

A receptor known as gC1qR/p32 is the primary site of binding for Lyp-1. The gC1qR/p32 mediates many biological events such as infection, inflammation and immune response. This receptor is abundantly expressed by endothelial cells localized in tumoral environment. It is proposed that the binding of Lyp-1 binds first to gC1qR/p32 is followed by cleavage into tLyp-1 that will subsequently bind on NRP-1 and/or NRP-2 and internalized into the targeted cells.¹²

In 2015, tLyp-1 was shown to be effective in delivering antitumor drugs towards gliomas. It was coupled with 5-carboxyfluorescein (FAM) or ¹⁸F-fluoride and the authors showed in U87MG glioblastoma cells xenografted in nude mice that the distribution of the targeted compounds in the tumor tissues of xenografted U87MG glioblastoma cells in nude mice was related to the expression of NRP-1.¹³ Very recently, a molecular modelling study of cyclic Lyp-1 in complex with its receptor gC1qR/p32 was performed by using a crystal structure of gC1qR/p32 from Protein Data Bank (PDB code: 1P32). It was shown that Asn3, Lys4, Arg5 and Arg7 were important amino acids for the specific binding of gC1qR/p32. The authors also supported their finding with molecular dynamic study, to further determine the interaction pattern between Lyp-1 and p32.¹⁴

As the truncated sequence of Lyp-1 produces tLyp-1 with a sequence of CGNKRTR that follows the CendR, we are of the opinion that it could be a useful candidate in the targeting of NRP-1 receptor. As far as we know, until now there is no docking simulation study being reported on the binding of tLyp-1 on NRP-1.

Previously in 2016, we published a molecular docking study of several peptides on NRP-1 receptor in combination with *in vitro* binding study, to determine the affinity of the tested peptides on this receptor and to explain the binding through in-depth simulation analysis.¹⁵ In this current study, similar approach of combined *in silico* and *in vitro* analysis was conducted

to evaluate the binding of tLyp-1 on NRP-1 and the importance of each amino acid in the sequence, through a technique called alanine-scanning (Ala-scan). A docking simulation study, a ligand binding assay and a 70 ns molecular dynamic (MD) simulation study were conducted on tLyp-1 and its Ala-scan analogues. The information presented in this paper will give an insight on the ability of this peptide to interact with NRP-1 receptor, and to confirm the amino acid(s) residue(s) that is/are important for the interaction. This will allow careful and guided manipulation of the peptide in the future for drug targeting towards NRP-1 receptor.

2. Materials and methods

2.1. Molecular docking simulation and ADMET predictions

The crystal structure of human NRP-1 (PDB ID: 6TKK) was retrieved from the Protein Data Bank database.^{16,17} Using Biovia Discovery Studio Visualizer, all water and heteroatoms were removed.¹⁸ Additional treatment on the crystal structure, such as reconstructing missing atoms, assigning atomic charges, and radii using the SWANSON force field (AMBER ff99 charges with optimised radii) was performed on the PDB2PQR web service (<https://pdb2pqr.poissonboltzmann.org/pdb2pqr>, accessed on June 14th, 2021).¹⁹ Protonation at pH 7.4 was carried out using (PROPKA3).^{20,21} The MolProbity web service (<http://molprobity.biochem.duke.edu/>, accessed on June 14th, 2021) was used for correction of bad contacts, the addition of missing hydrogen atoms and flipping of HIS, GLU, and ASN residues.^{21,22}

The new peptides (ligands) were sketched using the BIOVIA Discovery Studio Visualizer, and the ionizable side chains were protonated and corrected with the PROPKA3 tool pH 7.4 and MolProbity web service, as described above. Then, their geometries were optimized by UCSF Chimera 1.13 using steepest descents and conjugate gradient algorithms, with the termination conditions set to 1000 and 100 cycles, respectively, and the charge for minimization was assigned for the residues using AMBER ff14SB (UCSF Chimera 1.13 tool), and finally saved in PDB format.^{23,24}

Both the peptides and NRP-1 receptor were prepared for docking using MGLTools 1.5.6.²⁵ Kollman charges were added to all PDB files (peptides and protein) and saved in PDBQT format. Peptide flexibility (active rotatable bonds) was preserved. AutoDock-Crank Pep (ADCP)²⁶ was utilized to simulate the docking process, where the centre of grid box coordinates was set at $x = -5.780$, $y = -12.974$, $z = 19.468$ with the box size set to 25, 25, 25 (x , y , and z) by Auto site 1.1, padding= 4.0 Å, spacing 0.375 Å, smoothing = 0.5, number of replicas =100, and number of steps were set to 600000. The peptides' molecular interactions with the NRP-1 binding site were visualized and analyzed using BIOVIA Discovery Studio Visualizer, PyMol v.1.8.4.0,²⁷ and UCSF Chimera v. 1.13.²³

The ADMET properties were predicted using the ADMETlab 2.0 web service tool (<https://admetmesh.scbdd.com/service/evaluation/cal> (accessed on August 28, 2022)), which anticipates mutagenicity (Ames test), carcinogenicity, BBB permeability, and many other characteristics such as human intestinal absorption and plasma protein binding.²⁸ The two-dimensional chemical structures of all peptides were converted to SMILES format and submitted to the web tool for property prediction.

2.2. Molecular dynamic simulation

The best-docked conformation pose of tLyp-1 and its mutated analogue complexes with the NRP-1 binding site were used as the starting structure for a 70 ns molecular dynamic (MD) simulation. AMBER 18 was used for MD simulations.²⁹ The AMBER ff14SB force field was applied to the protein and peptides. The systems were solvated by dipping it in an octahedral box of TIP3P water, where the distances between the protein edge and the box were 8 Å, and

the system was neutralized by adding counter ions (chlorine Cl⁻), and the recorded are presented in Table 1.

Table 1. MD system setup details.

NRP-1 complexes with	Total Number of Atoms	Number of Peptide atoms	Water Atoms	Neutralizing Atoms
CGNKRTR	24268	118	21644	4 Cl ⁻
CGNKRTA	22141	104	19532	3 Cl ⁻
CGNKRAR	22314	114	19694	4 Cl ⁻
CGNKATR	21883	104	19274	3 Cl ⁻
CGNARTR	21702	106	19091	4 Cl ⁻
CGAKRTR	22797	114	20177	4 Cl ⁻
CANKRTR	23107	121	20480	4 Cl ⁻
AGNKRTR	21885	117	19262	4 Cl ⁻

The simulation protocol consisted of three minimization steps, whereby the first step includes 5000 cycles of conjugate gradient, 2000 for the second, and 1000 for the third step, with periodic boundary conditions at constant volume to eliminate the collision contacts between the macromolecule and the solvent, and to relax the system.^{21,30} The system was then gradually heated in three steps from 0-310 K for 1 ns, on all backbone atoms in each step using the Langevin dynamics thermostat with a coupling time of 0.2 ps. During the heating process, the NVT ensemble was used. Next, the equilibration of the protein atoms and the surrounding solvent was performed in three steps for 2 ns each, and the SHAKE algorithm³¹ was also utilized to constrain all bonds involving hydrogen.²¹

MD simulation was carried out until 70 ns. Trajectory analysis was done using CPPTRAJ to inspect the Root Mean Square Deviation and Fluctuation (RMSD and RMSF) values, radius of gyration (Rg) and hydrogen bond (H-bond) that were involved in the interaction between each ligand and the protein. QtGrace 0.2.6 was used to illustrate their graphs. Free binding energy and its energetic components for each system were collected for every 1 ps (total 1000 snapshots) from the last 1 ns of the trajectory using the MM-PBSA.py module in AMBER 18, and the data was calculated based on the "PBSA" model³² with a salt concentration of 0.150 M, to give a closer approximation to the true molecular volume, albeit in an average sense. In addition, the binding energy of the important amino acids was also calculated for the same region (69-70 ns; 1000 frames) using the MM-PBSA per residue decomposition scheme 2 (Per-residue decomp with 1-4 EEL added to EEL and 1-4 VDW added to VDW potential terms),³³ which will help in understanding the energetic effects and contributions of the residues in each system, all the equations are described in details.^{21,30}

2.3. Chemicals and materials

Ultrapure water (Milli-Q, $\rho > 18 \text{ M}\Omega\cdot\text{cm}$) was used in all the experiments. Acetonitrile (ACN), dichloromethane (DCM), dimethylformamide (DMF) and ethanol (EtOH) were obtained from Sigma-Aldrich and were used without further purification.

The synthesis of all peptides required *N,N,N',N'*-Tetramethyl-*O*-(*1H*-benzotriazol-1-yl)uronium hexafluorophosphate (HBTU) (Iris Biotech GmbH, Germany), acetic anhydride and piperidine (Sigma-Aldrich, Germany) and *N*-methylmorpholine (NMM), *N*-methylpyrrolidinone (NMP) (Alfa Aesar, Haverhill, MA, USA) as reagents. Fmoc-*L*-Cys(Trt)-OH, Fmoc-*L*-Lys(Boc)-OH, Fmoc-*L*-Gly-OH, Fmoc-*L*-Thr(tBu)-OH and Fmoc-*L*-Arg(Pbf)-OH were obtained from Iris Biotech GmbH (Germany). Fmoc-*L*-Ala-Wang resin (100-200 mesh), Fmoc-*L*-Arg(Pbf)-Wang resin (100-200 mesh) and Fmoc-*L*-Asn(Trt)-OH were obtained from Novabiochem (Germany). Trifluoroacetic acid (TFA) was purchased from Sigma Aldrich (Germany) and triisopropylsilane (TIPS) from Alfa Aesar (Haverhill, MA, USA).

2.4. Instruments

The peptides were synthesized using an automated ResPepXL peptide synthesizer (Intavis AG, Bioanalytical Instruments) and operated with a Multiple-Parallel Peptide Synthesis Program and were purified by HPLC using Shimadzu LC-20AT, column TSK gel amide-80 (3 μ m, 300 x 7.8 mm) equipped by an UV photodiode array detector (SPD-M20A). The UV detection was performed at 214 nm. The analysis by HPLC were performed using the same equipment with a column TSK gel amide-80 (3 μ m, 150 x 4.6 mm).

^1H NMR spectra were recorded on a Bruker Advance III 400 MHz spectrophotometer. The spectra were recorded in DMSO- d_6 at room temperature ($T = 298$ K) and residual peak of DMSO ($\delta = 2.5$ ppm) was used as internal reference. The chemical shifts (δ) are given in parts per million (ppm). High resolution mass spectrometry (HRMS) experiments were performed on a microTOF Bruker (electrospray ionization ESI+, 50–1000 in low and 50–2500 in width).

2.5. Synthesis

All the peptides were synthesized using the automated ResPepXL peptide synthesizer, according to a classical Fmoc/tBu solid phase methodology at 50 μ mol scale. The side chains of arginine (Arg, R), asparagine (Asp, N), cysteine (Cys, C), lysine (Lys, K) and threonine (Thr, T) were protected by Pbf, Trt, tBu or Boc groups (see 2.3. section). A Fmoc-*L*-Arg(Pbf)-Wang resin or Fmoc-*L*-Ala-Wang resin was used as the starting material and swelled in DCM. The Fmoc groups were removed by piperidine (20% in DMF). This step was performed three times, first, during 4 min and the next two for 7 min. The next amino acid was then grafted with the coupling step by adding an excess of Fmoc-aminoacid-OH (6 eq), HBTU (5 eq), NMP (3 eq) and NMM (10 eq) in DMF. This step was repeated two times for 18 min and three times for the last amino acid. A last step of capping, using a solution of acetic anhydride (5% in DMF), was performed for 5 min, to trap all functions that did not react. The process of deprotection, coupling and capping were repeated until the desired sequences of amino acids were grafted on the resin. At the end of each step, all soluble reagents on the resin and the protecting group at the *N*-terminus of the peptide were removed by filtration and washing process with DCM, EtOH and DMF. The final Fmoc protection was removed using piperidine performed 4 times for 15 min. The resin was dried under vacuum and then cleaved (with full deprotection of lateral chains) using TFA/TIPS/water (92.5/2.5/5; v/v/v) for 2 h. The acidic resin was filtered and washed with TFA and DCM. The filtrate was dried under vacuum and the compound was precipitated in diethylether by centrifugation. The crude product was further purified by semi-preparative HPLC using ACN/H₂O (0.1% TFA; 95/5) to 55% ACN gradient in 25 min, followed by isocratic ACN for 10 min at a flow of 1.7 mL/min. tLyp-1 and its 7 Ala-scan analogues were obtained with an HPLC purity up to 95% and characterized by 1D and 2D NMR (^1H , COSY and TOCSY) and HRMS experiments (see Supporting Information, Tables S1-S8).

2.6. Biological test-binding study of the peptides on recombinant NRP-1 receptor

The affinity of peptides for NRP-1 was assessed as previously described.⁵⁻⁹ Briefly, the surface of the high protein-binding capacity polystyrene 96 well ELISA plate (NUNC MaxiSorp™, Sigma-Aldrich, France) was coated with NRP-1 at a concentration of 2 μ g/mL in phosphate buffer saline (PBS) and kept overnight at room temperature. The plate was then blocked with a solution of PBS containing 0.5% bovine serum albumin (BSA) during 1 h at 37°C, to inhibit non-specific interactions. Binding of the tested peptides to NRP-1 was evaluated using 5 ng/mL of biotinylated VEGF-A₁₆₅ in blocking buffer containing 2 μ g/mL of heparin. Biotinylated VEGF-A₁₆₅ was added to the coated wells, in competition, or not, with different concentration of peptide. The plates were further incubated for 2 h at room temperature. After that, the plates were washed 3 times with a solution of PBS containing 0.05% Tween 20 and the amount of bound biotinylated VEGF-A₁₆₅ was assayed as it was stained with

streptavidin horseradish peroxidase conjugate and its substrate (tetramethylbenzidine and H₂O₂). After 20 min of incubation at room temperature, the reaction was stopped by the addition of 2N sulfuric acid (i.e., final sulfuric acid concentration of 0.65N). The corresponding optical densities were then measured at a wavelength of 450 nm. The obtained results were expressed as relative absorbance to wells containing only blocking buffer. For this assay, three wells were used per condition.^{1,17}

3. Results and Discussion

3.1. Molecular docking and ADMET predictions

At the time of initiating this study, there were 24 NRP-1 crystal structures (see Supporting Information, Table S9) deposited in the RCSB Protein Data Bank (PDB).^{17,34-46} Of these structures, 20 were of *homo sapiens* (human origin), 2 were of *rattus norvegicus* (rat), and 2 *mus musculus* (mouse). The crystal structure of the NRP-1-b1 domain (PDB code: 6TKK) bound to the C-terminal peptide (Ace-Arg-Pro-Gln-Pro-Arg) was chosen for this study (Figure 1). Despite not being the structure with the lowest resolution, it is however the most recent NRP-1 structure in the PDB bound with a peptide. Furthermore, the bound pentapeptide might give some insights on the binding of a peptide in NRP-1-b1 binding site. In the crystal structure, Ace-RPQPR, which possesses a C-terminal CendR sequence, was found to interact with NRP-1-b1 key binding site residues such as Tyr297, Asp320, and Ile415 *via* ionic interactions and/or hydrogen bonds between the guanidine moiety of the C-terminal Arg and the carboxylic acid moiety of these residues. Also, Trp301 and Tyr353 created hydrophobic interactions with the alkyl chain of the C-terminal Arg. Proline (Pro) residues participated in the interactions through creating H-bonds and hydrophobic interactions with Tyr297.

Figure 1 shows the superimposition of the crystal structure and the re-docked conformation of Ace-RPQPR on NRP-1 (PDB ID: 6TKK). Re-docking was done using molecular docking software AutoDock Crank Pep (ADCP).²⁶ ADCP is a *de novo* method for protein-peptide docking that folds the peptide in the potential energy landscape created by a given receptor. It combines CRANKITE's conformation sampling ability with the grid-based AutoDock representation of a rigid receptor.²⁶ AutoDock, and its current version 4.2 is a popular molecular docking program but is known to have limitations in docking peptides longer than 5 sequences with more than 32 rotatable bonds.⁴⁷⁻⁴⁹ ADCP on the other hand is purposely developed for protein-peptide docking and it can treat flexible peptides with up to 20 amino acids into rigid receptors,²⁶ thus overcoming the current limitation of peptide docking using AutoDock. From Figure 1, Ace-RPQPR is seen to docked at the VEGF₁₆₅ binding site in almost the same conformation as its crystal structure with an RMSD of 2.7 Å. As the NRP-1 b1 binding pocket is shallow, it was reported that only the terminal Arg of a ligand will be able to directly enter and interact with the pocket.⁵⁰⁻⁵² As can be seen in the figure, both the crystal and re-docked structures entered the pocket from the terminal Arg and maintain the interactions with key residues Tyr297, Trp301, Asp320 and Tyr353. However, the re-docked Ace-RPQPR lost its H-bond interaction with Ile415.

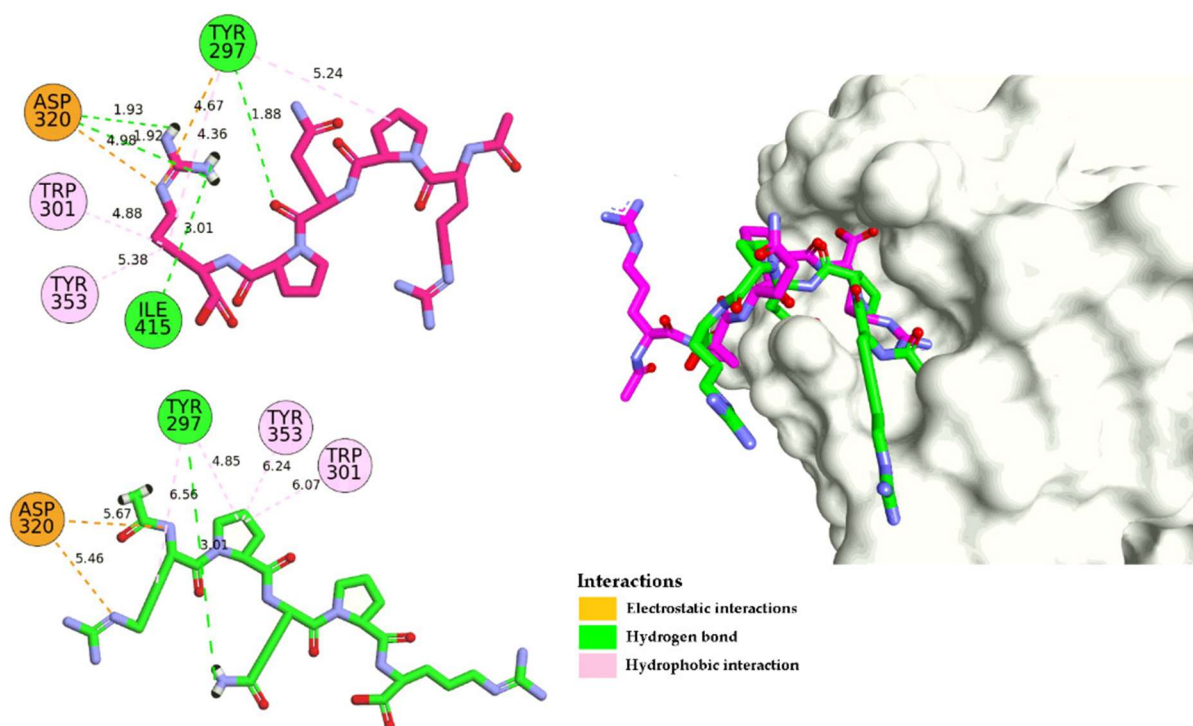


Figure 1. Superimposition of the crystal structure of Ace-RPQPR (C pink, O red, and N blue) and the docked model (C green, O red, and N blue) on neuropilin-1 (NRP-1) crystal structure (PDB ID: 6TKK) with RMSD = 2.7 Å and their 2D interactions into the binding site. These models were generated using the Discovery Studio visualizer.

CendR or C-end rule sequence is important for the binding of a peptide ligand to NRP-1.⁴⁵ A previous study by Teesalu *et al.* (2009) on the screening of phage libraries identified a R/K-XX-R/K motif to be important in the interaction of a ligand with NRP-1.⁵² Many peptides targeting NRP-1 have the CendR fragment in the sequence, and this includes the C-terminus of VEGF₁₆₅ (GDKPRR). Based on the literature data, the key amino acids in NRP-1 that are important in its binding interaction and inhibition include Tyr297, Thr316, Asp320, Ser346, Thr349, and Tyr353.^{24,35,43,53}

The docking scores (ΔG_{bind}) of tLyp-1 (CGNKRTR, **1**) and the 7 Ala-scan analogues (**2-8**) are given in Table 2. The results revealed that all of the heptapeptides interacted with the NRP-1 binding site significantly with similar binding affinity considering that the docking errors are approximately ± 2 kcal/mol. All peptides that have C-terminal Arg residues with the exception of CGNARTR (**5**) showed relatively higher binding affinity compared to CGNKRTA (**2**) although the scores are not significantly different. Analysis of the binding interactions of the peptides with NRP-1 also showed that the peptides more or less bind at the same binding site with residues Gly318, Asp320, Glu348 and Lys351 (Figure 2). Since the binding affinities predicted by docking are not significantly different, we decided to conduct 1) the synthesis and *in vitro* IC₅₀ determination of all peptides **1-8** for NRP-1 (see 3.2. and 3.3. sections), and also 2) MD simulations to have more in-depth understanding of the interaction (see 3.4 section). The docked conformations were taken as the starting structures for MD simulations.

Table 2. The docking scores for tLyp-1 (CGNKRTR, **1**) and its 7 Ala-scan analogues (**2-8**) against NRP-1 (6TKK.PDB) using ADCP.

Peptide No.	Peptide sequence	ΔG_{bind} (Kcal/mol) ^a	Experimental IC ₅₀ ^c
-------------	------------------	--	--

1	CGNKRTR	-12.30	4 ± 2 μM
2	CGNKRTA	-11.90	ND
3	CGNKRAR	-12.40	4 ± 1 μM
4	CGNKATR	-12.60	18 ± 1 μM
5	CGNARTR	-10.90	50 ± 2 μM
6	CGAKRTR	-12.20	7 ± 1 μM
7	CANKRTR	-12.10	3 ± 1 μM
8	AGNKRTR	-12.50	4 ± 1 μM
-	Ace-RPQPR ^b	-5.70	-

^a Binding affinity predicted by AutoDock Crank Pep.

^b Ace-RPQPR is the co-crystallized ligand in 6TKK.PDB.

^b Experimental IC₅₀ obtained using ligand binding assay (see 3.3. section).

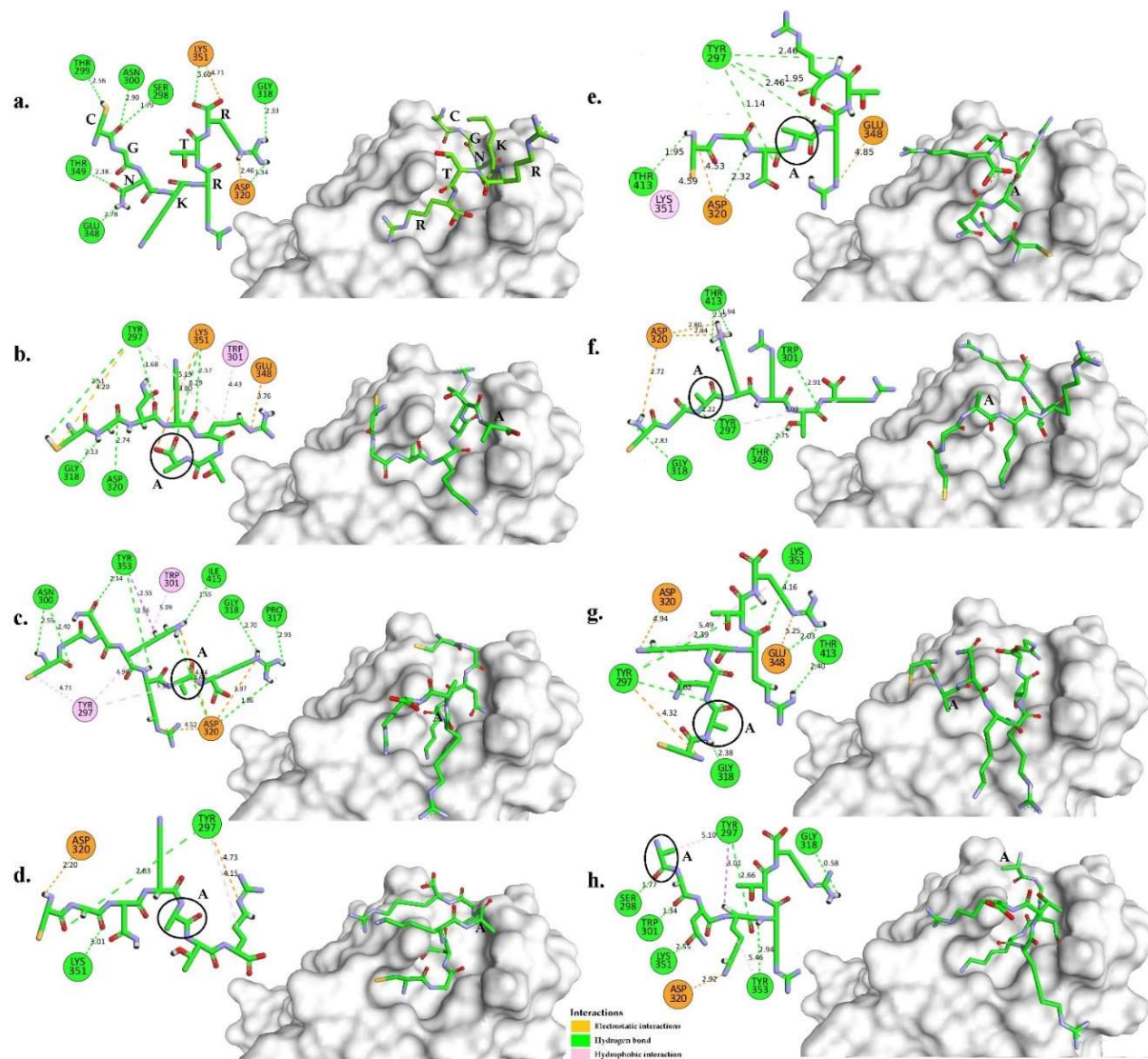


Figure 2. Poses of docked peptides interacting with NRP-1 binding site residues: (a) CGNKRTR (tLyp-1, **1**), (b) CGNKRTA (**2**), (c) CGNKRAR (**3**), (d) CGNKATR (**4**), (e) CGNARTR (**5**), (f) CGAKRTR (**6**), (g) CANKRTR (**7**), and (h) AGNKRTR (**8**). The peptides are rendered stick (C in green, O in red, and N in sky blue). Ionic bonds, hydrogen bonds, and hydrophobic interactions between the peptides and the residues are shown as orange, green, and pink dashed lines, respectively. The alanine residue was highlighted in a black circle and with its one letter code.

Early predictions of physicochemical properties like absorption, distribution, metabolism, excretion, and toxicity (ADMET) have become a prime/ fundamental consideration to reduce the chances of drug failure at the clinical level.⁵⁴⁻⁵⁶ With this aim, the

	CYP2D6 substrate	No							
	CYP1A2 inhibitor	No							
	CYP2C19 inhibitor	No							
	CYP2C9 inhibitor	No							
	CYP3A4 inhibitor	No							
Excretion	CL (Clearance Rate) mL/min/kg	1.02	1.17	0.88	1.32	1.04	1.24	0.97	0.89
	T $\frac{1}{2}$ (Half Lifetime) hr	0.81	0.80	0.41	0.80	0.80	0.85	0.78	0.81
Toxicity	hERG (hERG Blockers)	-	-	-	-	-	-	-	-
	H-HT (Human Hepatotoxicity)	-	-	-	-	-	-	-	-
	AMES (Ames Mutagenicity)	-	-	-	-	-	-	-	-

Papp Caco-2 Permeability (Optimal: higher than -5.15 Log unit or -4.70 or -4.80); HIA (>30%: HIA is +ve; <30%: HIA is -ve) +ve: greater affinity, -ve values: low affinity, PPB (90% Significant with drugs that are highly protein-bound and have a low therapeutic index); BBB (BBB ratio ≥ 0.1 : BBB+; BB ratio <0.1: BBB-); T $\frac{1}{2}$ (>8 h: high; 3 h – 8 h: moderate; <3 h: low); CL (>15 mL/min/kg: high; 5 mL/min/kg <CL <15 mL/min/kg: moderate; <5 mL/min/kg: low). -ve values mean low affinity while +ve values indicate greater affinity.

3.2. Synthesis and characterization of the peptides

The peptides CGNKRTR (tLyp-1, **1**) and its 7 Ala-scan analogues (CGNKRTA (**2**), CGNKRAR (**3**), CGNKATR (**4**), CGNARTR (**5**), CGAKRTR (**6**), CANKRTR (**7**), AGNKRTR (**8**)) were synthesized on solid phase and purified by HPLC leading to a final purity superior to 95%. The successful synthesis of the peptides was confirmed by 1D and 2D NMR (^1H , COSY and TOCSY) and HRMS experiments (see Supporting Information, Tables S1-S8). The ^1H NMR spectra revealed, for all the peptides of Ala-scan containing the Gly, a doubling of the signal of NH^α of this last amino acid indicating the existence of two conformations for this amino acid. Surprisingly, this doubling of the signal was not observed for the original peptide, indicating a change in the conformation of the peptide. Moreover, at this same position, when the Gly was replaced by an Ala, only one signal was observed for NH^α . The signal corresponding to the NH^α of the Cys was not observed probably due to the position *N*-terminal of this amino acid and thus a protonation of this amine function for all the peptides.

3.3. In vitro affinity for NRP-1

The *in vitro* affinity of the peptides **1-8** was determined using ligand binding assay (LBA). VEGF₁₆₅ has a high affinity for NRP-1⁶³ and was chosen as a competitor of the synthesized peptides (Figure 3). Our developed NRP-1-targeted peptide (KDKPPR)⁵⁻⁹ was used as reference. We observed a similar value of IC_{50} for KDKPPR (1 μM) and tLyp-1 (**1**, 4 μM), indicating the efficient potential of tLyp-1 for NRP-1 targeting. The results highlighted that the *C*-terminal Arg is essential for the affinity of NRP-1 (CGNKRTA (**2**), IC_{50} not determined) according to the CendR motif. Moreover, the importance of the other Arg and the Lys was also observed (CGNKATR (**4**, 18 μM) and CGNARTR (**5**, 50 μM), respectively). However, it appeared that the Cys and the Gly are not involved in the good affinity of the tLyp-1 for NRP-1 (AGNKRTR (**8**, 4 μM) and CANKRTR (**7**, 3 μM), respectively).

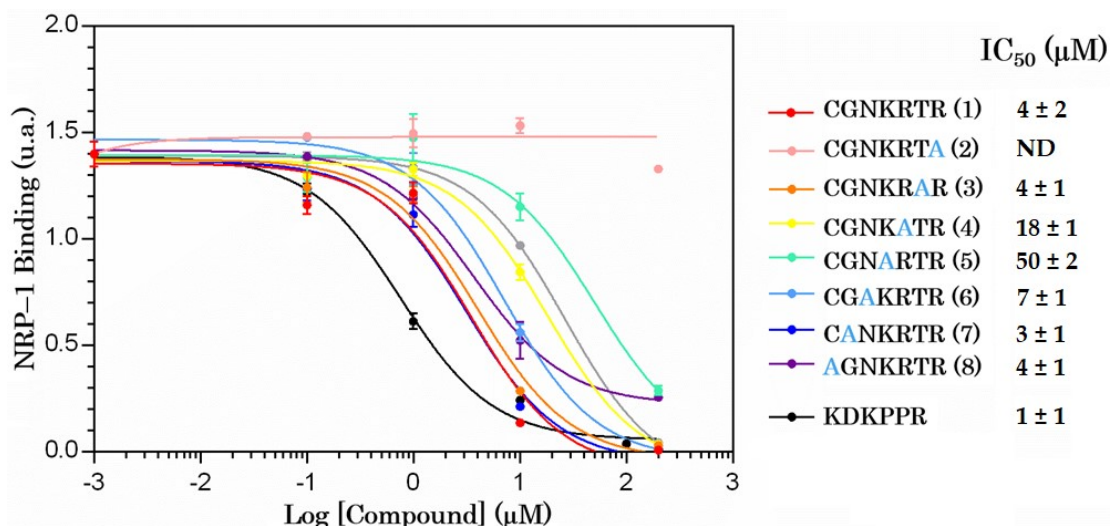


Figure 3. NRP-1 binding of peptides obtained using a competitive binding assay.

3.4. MD Simulation

3.4.1 Stability of the simulated systems

VEGF₁₆₅/NRP-1 has been known to be involved in cancer pathology and it is an example of protein-protein interaction (PPI) which can be exploited in new anti-cancer drug discovery.⁶⁴⁻⁶⁶ Drug discovery targeting PPI is known to be challenging. One of the challenges is the large and shallow PPI interfaces which render difficulty for ligand binding. Although NRP-1 has many PPIs sites, the binding site for VEGF in b1 domain is also quite shallow.⁵⁰ Figure 1 shows the binding site of Ace-RPQPR which was used to dock tLyp-1 and its Ala-scan analogues (see 3.1. section). Following docking (see 3.1. section), we carried out 70 ns MD simulations of NRP-1 in complex with tLyp-1 (**1**) and its Ala-scan analogues (**2-8**) to understand further the significance of each residue of tLyp-1 towards the binding interaction. Figure 4 showed the root mean square deviation (RMSD) plots of the backbone of NRP-1 and the peptide ligands' complex systems. In general, for the NRP-1 backbone, all systems showed average RMSDs between 1.90 – 2.43 Å, while the peptides ligand showed average RMSDs between 2.08 to 4.45 Å. The results indicate high flexibility of the peptides compared to the protein. Substitution with Ala at the *N*-terminal (AGNKRTR, **8**) resulted in highest flexibility amongst the peptides. Interestingly, CGNKRAR (**3**) showed least flexibility with RMSD = 2.08 Å and with the NRP-1 also showed low RMSD = 2.0 Å. As a comparison, the apo-NRP-1 system showed an average RMSD = ~ 2.22 Å indicating a stability of the system throughout the 70 ns.

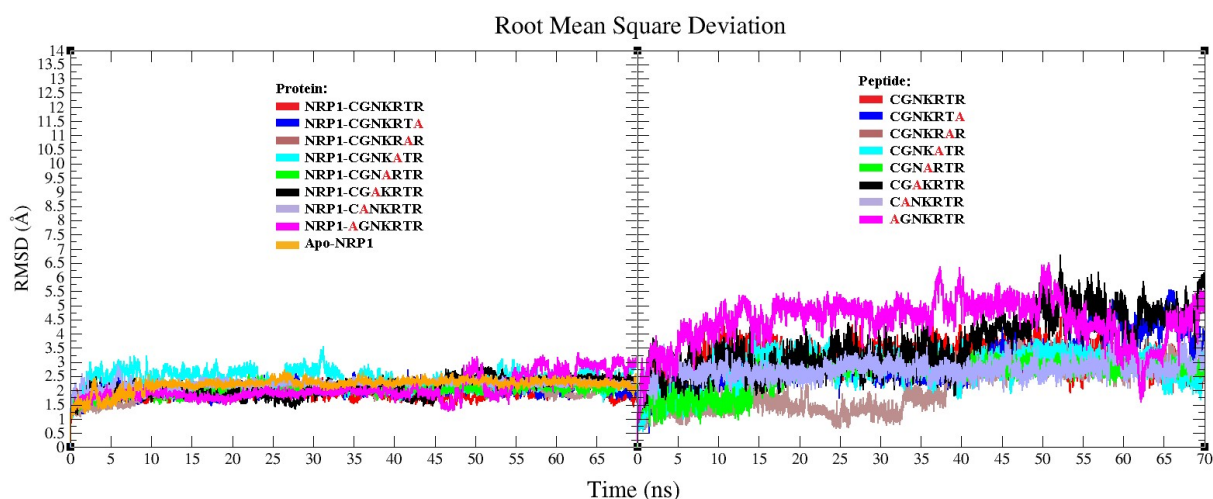


Figure 4. The root mean square deviation (RMSD) plots of the protein and peptide backbones for all systems over all 70 ns of MD simulation time.

Figure 5 (a and b) showed an estimated measure of flexibility using Root Mean Square Fluctuation (RMSF) for residues in all the 9 systems. There are generally some similarities in all the systems with some regions showing minimal residues fluctuation (within 1.0 Å). Regions 315-325, 345-352, 373-379 show slightly more pronounced residue fluctuations (1.5 – 2.0 Å), as shown in Figure 5a. It is interesting to note that residue Asp20 in the apo-system showed the highest fluctuation but in the holo systems this residue only showed minimal fluctuation. NRP-1-CGDKRTR (2) system in general demonstrated slightly higher fluctuations in all regions compared to other analogues, however, the differences are not very significant (Figure 5a). Interestingly, Figure 5b shows that the backbone residues of three of the mutated peptides (CGAKRTR (6), CGNARTR (5), and CGNKATR (4)) are significantly more stable and less mobile (less than 2 Å) compared to the tLyp-1 (1) and its resting mutated analogues, indicating that it maintained its conformations throughout the MD simulation time. In addition, substituting the *N*-terminal Cys by Ala (AGNKRTR, 8) has a drastic effect on the stability of the AGNKRTR backbone, particularly on the Lys and Arg residues, where it was shown to fluctuate more than the tLyp-1 in an average of 3 Å.

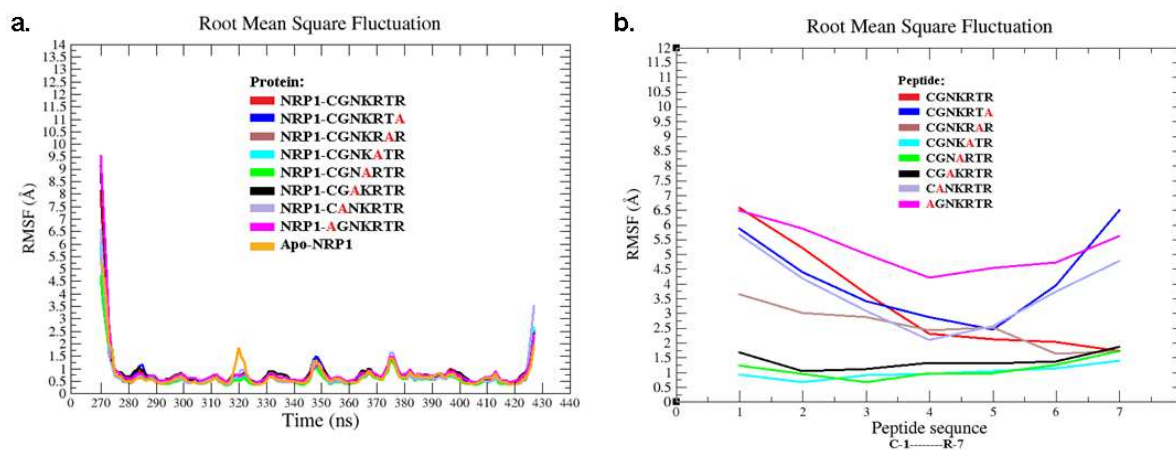


Figure 5. The root mean square fluctuation (RMSF) plots of the NRP-1 backbone atoms (a) for all systems, and (b) for the peptides, throughout the 70 ns MD simulation time.

The time evolution of the radius of gyration (R_g) of NRP-1 in all the systems (Figure 6) showed that the values of R_g fluctuates between 15.0–15.5 Å, indicating that the protein in all systems remains compact and no significant expansion in the structures can be observed.

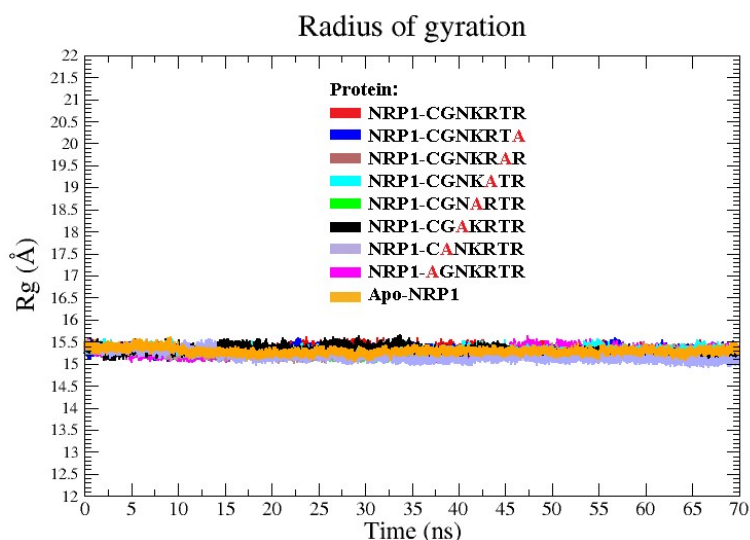


Figure 6. Radius of gyration (R_g) graphs of the NRP-1 backbone atoms of all systems over the MD interval time (0–70ns).

3.4.2. Hydrogen bond (H-bond) analysis

H-bonds contribute to the stability of the protein secondary structures and protein interaction with the ligands.^{21,30} In this work, the H-bond occupancy and frequency (lifetime max) were analyzed for tLyp-1 (CGNKRTR, **1**) and its 7 Ala-scan analogues (**2-8**) into the binding site of NRP-1 throughout the MD simulation (0-70 ns). Tyr297, Thr316, Asp320, Ser346, Thr349, and Tyr353 have been reported as the key amino acids in the active site and binding with them could enhance the inhibition of the receptor.^{24,35,43,53} The H-bonds were divided by their percentage of occupancy into strong (more than 60%), moderate (between 30–60%), and weak hydrogen bonds (that occupied 10–30%) during the MD simulation.^{21,30}

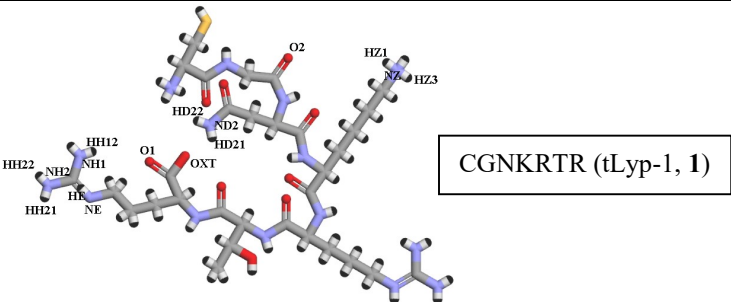
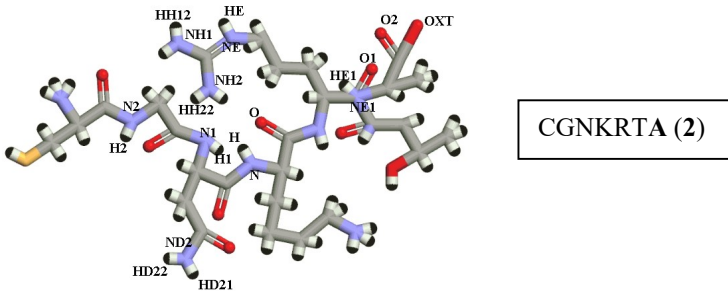
The results revealed a variation in the tendency of H-bond formation between t-Lyp1 and its Ala-scan analogues with NRP-1 binding site, especially with the key amino acid Asp320 (Table 4). From the MD simulation conducted, it can be seen that the Arg residue at the C-terminus of the peptide in the CGNKRTR-NRP-1 system exhibited two strong hydrogen bonds: one with Asp320 at high-frequency (613 time) and one with Pro317 at low frequency (61 time) with occupancies of 97.37% and 80.95%, respectively. The Arg residue (C-terminus) of CGNKRTR (t-Lyp1, **1**) also formed four moderately strong H-bonds with Asp30, Pro317, and two bonds with Tyr353 with an average occupancy of 48.25%, 47.83%, 41.70%, and 41.52%, respectively (Table 4). Two of the H-bonds exhibited a relatively high frequency of occurrence, (i.e., those formed by Tyr353 (488 and 505 times)). Other H-bond interactions between CGNKRTR (t-Lyp1, **1**) and NRP-1 binding site residues were also created but comparatively weaker.

As expected, substituting the C-terminus Arg residue of t-Lyp1 with Ala (CGNKRTA, **2**) has led to a reduced H-bond occupancy with Asp320 (OD1) to approximately half of the occupancy recorded by Arg (56.33%). The absence of Arg at the C-terminal has also diminished several weak H-bonds between the peptide and NRP-1, such as those with Lys351 and Tyr353. However, there is still H-bond interaction between the peptide and Tyr353, which was formed between Lys-4 and Arg-5 instead.

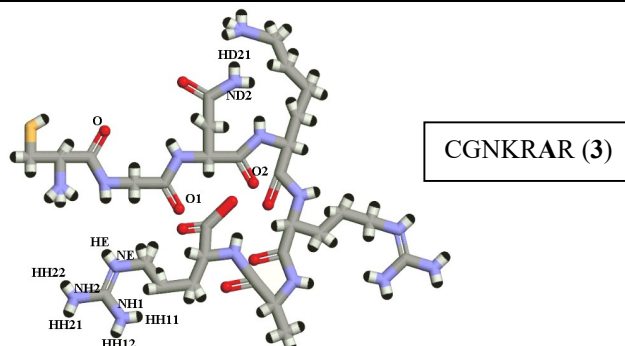
It is worth noting that the Arg residue at the C-terminus of CGNKRAR (**3**) formed a strong H-bond with OD2 atoms of Asp320 at a high frequency (261 time) with an occupancy of ~71%, whilst a weaker interaction was recorded with OD1 of Asp320 (23% occupancy, 284 time). Moreover, it was also found that CGNKRAR (**3**) formed five moderate H-bonds, four of them with the Arg residue at the C-terminus, although with low frequency (<100 time).

Like CGNKRTA (2), mutating the Arg residue at position 5 (CGNKATR, 4) has an obvious effect on the H-bonds interaction, especially on the lifetime frequency. CGNKATR (4) formed three strong H-bonds with Tyr353 (~78%), Asp320 (73.31%), and Thr349 (65.74%), but all with low-frequencies (<100 time). CGNARTR (5) on the other hand maintained three strong H-bonds, however the frequency and lifetime were significantly reduced as compared to the native peptide tLyp-1. This analysis supports the importance of the Lys and Arg residues in the tLyp-1 sequence, as substituting Lys-4, Arg-5 and Arg-7 shows reduction in the H-bonds occupancy and/or frequency, in comparison to the native peptide tLyp-1.^{50,52,67}

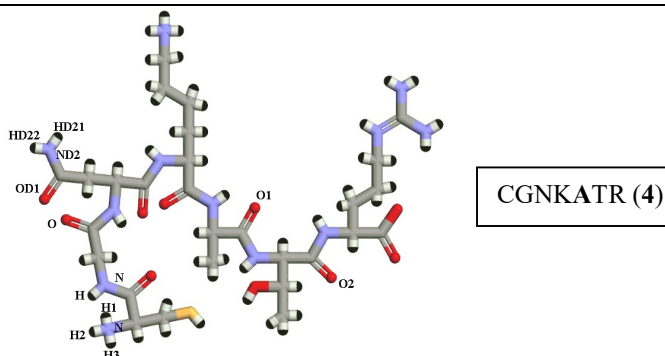
Table 4. The average H-bond occupancy and frequency (lifetime max) for the derived region of MD simulation (0-70 ns) for the CGNKRTR and its Ala-scan analogues. The interacted peptide residues are rendered in a red colour.

H-Bond Acceptor (atom@res)	Bond Donor (atom@res-H)	H-Bond occupancy (%)	Average Distance (Å)	Average Angle (°)	LifeTime (Max)
					
ASP320≅OD1	CGNKRT R ≅NH2-HH21	97.37	2.76	160.65	613
PRO317≅O	CGNKRT R ≅NH2-HH22	80.95	2.83	154.48	61
ASP320≅OD2	CGNKRT R ≅NE-HE	48.25	2.87	155.83	24
PRO317≅O	CGNKRT R ≅NH1-HH12	47.83	2.86	150.15	40
CGNKRT R ≅OXT	TYR353≅OH-HH	41.70	2.66	164.79	488
CGNKRT R ≅O1	TYR353≅OH-HH	41.52	2.67	164.94	505
CGNKRT R ≅O2	TYR297≅OH-HH	23.82	2.74	162.90	137
TYR353≅OH	CGNKRT R ≅ND2-HD21	17.60	2.89	159.99	24
ASP320≅OD1	CGNKRT R ≅NE-HE	16.70	2.89	144.89	11
CGNKRT R ≅OXT	LYS351≅NZ-HZ1	14.73	2.81	154.35	45
CGNKRT R ≅O	TRP301≅NE1-HE1	14.23	2.85	161.18	53
CGNKRT R ≅O1	LYS351≅NZ-HZ1	13.89	2.82	154.19	24
CGNKRT R ≅OXT	LYS351≅NZ-HZ2	13.57	2.81	154.53	66
CGNKRT R ≅O1	LYS351≅NZ-HZ3	12.87	2.81	154.23	39
CGNKRT R ≅O1	LYS351≅NZ-HZ2	12.84	2.81	153.97	29
CGNKRT R ≅OXT	LYS351≅NZ-HZ3	12.64	2.81	154.30	43
GLY318≅O	CGNKRT R ≅NZ-HZ1	10.54	2.81	155.98	42
GLU319≅OE2	CGNKRT R ≅NZ-HZ3	10.3	2.78	156.11	85
					
ASP320≅OD1	CGNKRTA≅ND2-HD22	56.33	2.80	160.63	141
ASP320≅OD2	CGNKRTA≅N-H	38.51	2.86	160.27	66
ASP320≅OD2	CGNKRTA≅NH1-HH12	19.98	2.77	156.60	315
CGNKRTA≅O	TYR353≅OH-HH	17.03	2.76	162.66	154
CGNKRTA≅O1	TYR353≅OH-HH	14.13	2.73	160.68	164

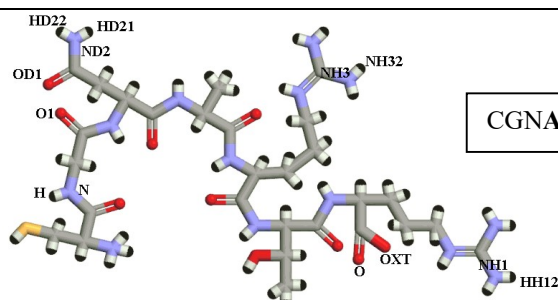
CGNKRTA \cong O2	THR349 \cong OG1-HG1	13.03	2.71	161.96	145
CGNKRTA \cong O2	SER346 \cong OG-HG	12.05	2.68	160.11	105
PRO317 \cong O	CGNKRTA \cong NE-HE	11.62	2.85	150.85	37
CGNKRTA \cong OXT	TRP301 \cong NE1-HE1	11.54	2.84	154.73	42
ASP320 \cong OD2	CGNKRTA \cong NH2-HH22	11.3	2.83	149.17	86
GLY318 \cong O	CGNKRTA \cong N1-H1	10.35	2.89	156.20	14
GLU319 \cong OE1	CGNKRTA \cong N2-H2	10.05	2.84	155.99	52



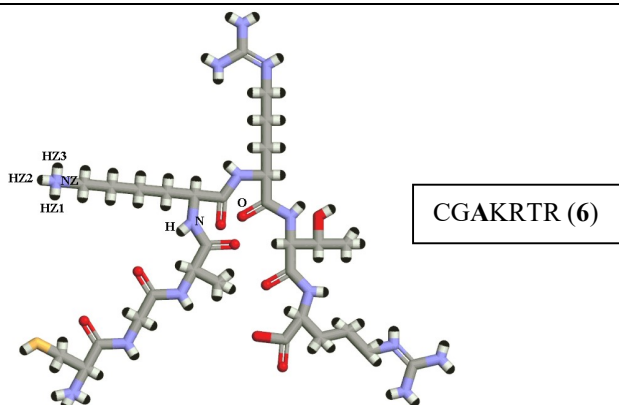
ASP320 \cong OD2	CGNKRAR \cong NH2-HH22	71.02	2.78	160.25	261
PRO317 \cong O	CGNKRAR \cong NH2-HH21	52.82	2.83	151.17	74
PRO317 \cong O	CGNKRAR \cong NE-HE	50.3	2.86	148.69	29
ASP320 \cong OD1	CGNKRAR \cong NH1-HH12	47.73	2.83	158.76	40
CGNKRAR \cong O1	ASN300 \cong ND2-HD21	45.45	2.84	156.43	50
ASP320 \cong OD2	CGNKRAR \cong NH1-HH12	31.45	2.84	154.43	31
CGNKRAR \cong O1	TRP301 \cong NE1-HE1	25.72	2.86	154.11	43
CGNKRAR \cong O	TYR297 \cong OH-HH	24.47	2.74	160.48	60
ASP320 \cong OD1	CGNKRAR \cong NH2-HH22	23.65	2.78	162.81	284
CGNKRAR \cong O1	SER298 \cong OG-HG	14.54	2.74	159.82	145
CGNKRAR \cong O2	TYR297 \cong OH-HH	12.78	2.76	160.82	66
TYR353 \cong OH	CGNKRAR \cong ND2-HD21	11.5	2.90	155.23	15
THR316 \cong OG1	CGNKRAR \cong NH2-HH21	10.8	2.86	146.88	8



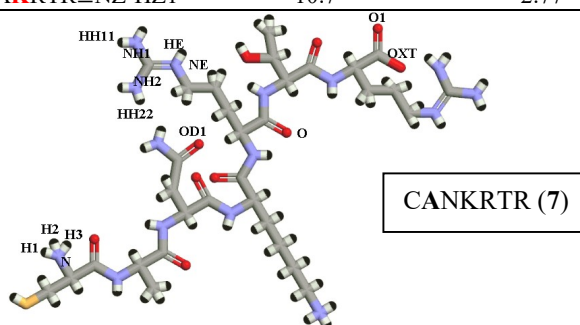
CGNKATR \cong O	TYR353 \cong OH-HH	78.01	2.78	163.73	55
ASP320 \cong OD2	CGNKATR \cong N-H	73.31	2.83	156.71	88
CGNKATR \cong O1	THR349 \cong OG1-HG1	65.74	2.77	164.77	91
ASP320 \cong OD1	CGNKATR \cong ND2-HD21	45.24	2.85	149.85	35
PRO317 \cong O	CGNKATR \cong ND2-HD22	43.2	2.83	148.75	25
ASP320 \cong OD2	CGNKATR \cong N-H2	28.34	2.80	155.71	69
ASP320 \cong OD2	CGNKATR \cong N-H1	27	2.80	155.57	67
ASP320 \cong OD2	CGNKATR \cong N-H3	24.75	2.80	155.51	48
CGNKATR \cong O2	SER346 \cong OG-HG	20.42	2.77	154.73	39
CGNKATR \cong OD1	ASP320 \cong N-H	10.61	2.90	149.99	9



ASP320 \cong OD1	CGNARTR \cong N-H	66.20	2.84	152.89	78
ASP320 \cong OD2	CGNARTR \cong ND2-HD21	63.57	2.82	152.88	84
CGNARTR \cong O1	TYR353 \cong OH-HH	62.67	2.73	161.44	95
PRO317 \cong O	CGNARTR \cong ND2-HD22	38.51	2.83	148.85	45
ASP320 \cong OD2	CGNARTR \cong ND2-HD22	19.03	2.76	163.96	305
CGNARTR \cong OD1	ASP320 \cong N-H	17.39	2.89	149.11	11
TYR353 \cong OH	CGNARTR \cong NH3-HH32	12.69	2.87	153.54	16
CGNARTR \cong O	LYS351 \cong NZ-HZ3	12.26	2.79	156.83	48
CGNARTR \cong O	LYS351 \cong NZ-HZ2	12.13	2.79	156.89	58
CGNARTR \cong O	LYS351 \cong NZ-HZ1	11.73	2.79	156.55	48
CGNARTR \cong OXT	LYS351 \cong NZ-HZ1	11.71	2.79	156.66	72
CGNARTR \cong OXT	LYS351 \cong NZ-HZ3	11.65	2.79	156.67	54
CGNARTR \cong OXT	LYS351 \cong NZ-HZ2	11.46	2.79	156.52	43
GLU319 \cong OE1	CGNARTR \cong NH1-HH12	10.01	2.80	157.62	61

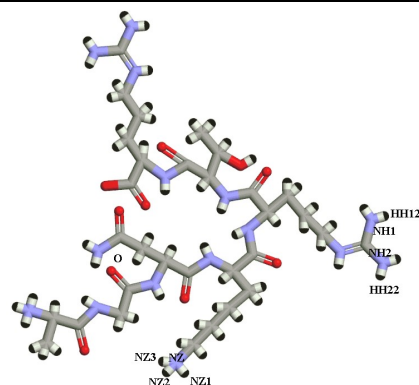


GLY318 \cong O	CGAKRTR \cong N-H	36.03	2.87	162.44	45
CGAKRTR \cong O	TYR297 \cong OH-HH	27.71	2.73	163.48	114
PRO317 \cong O	CGAKRTR \cong NZ-HZ1	23.34	2.81	157.66	67
PRO317 \cong O	CGAKRTR \cong NZ-HZ3	23.19	2.82	157.38	93
PRO317 \cong O	CGAKRTR \cong NZ-HZ2	19.23	2.82	157.56	49
ASP320 \cong OD1	CGAKRTR \cong NZ-HZ2	16.98	2.77	159.33	116
ASP320 \cong OD2	CGAKRTR \cong NZ-HZ3	15.48	2.76	158.45	241
ASP320 \cong OD1	CGAKRTR \cong NZ-HZ3	15.35	2.77	158.66	156
ASP320 \cong OD2	CGAKRTR \cong NZ-HZ2	13.14	2.76	157.50	166
THR316 \cong OG1	CGAKRTR \cong NZ-HZ2	11.49	2.83	151.91	69
ASP320 \cong OD1	CGAKRTR \cong NZ-HZ1	11.37	2.77	158.29	145
ASP320 \cong OD2	CGAKRTR \cong NZ-HZ1	10.7	2.77	157.80	144



ASP320 \cong OD1	CANKRTR \cong NE-HE	63.21	2.82	155.35	62
CANKRTR3 \cong O	TYR353 \cong OH-HH	51.8	2.74	162.87	88

THR_144 \cong O	CANKRTR \cong NH1-HH11	47.85	2.83	156.68	60
ASP320 \cong OD1	CANKRTR \cong NH2-HH21	25.02	2.82	149.76	52
ASP320 \cong OD1	CANKRTR \cong N-H2	16.58	2.80	151.76	30
ASP320 \cong OD1	CANKRTR \cong N-H1	16.51	2.80	152.35	29
CANKRTR \cong O1	LYS351 \cong NZ-HZ3	15.23	2.79	156.23	48
CANKRTR \cong OD1	TYR297 \cong OH-HH	14.96	2.74	162.82	56
CANKRTR \cong O	LYS351 \cong NZ-HZ1	14.52	2.79	156.00	57
ASP320 \cong OD1	CANKRTR \cong N-H3	13.75	2.80	151.92	23
CANKRTR \cong O1	LYS351 \cong NZ-HZ2	12.32	2.79	155.49	47
CANKRTR \cong OXT	LYS351 \cong NZ-HZ3	11.96	2.79	155.61	43
CANKRTR \cong OXT	LYS351 \cong NZ-HZ1	11.43	2.80	155.28	67
CANKRTR \cong OXT	LYS351 \cong NZ-HZ2	10.86	2.80	155.35	31
CANKRTR \cong OXT	THR349 \cong OG1-HG1	10.67	2.71	165.43	119
ASP320 \cong OD2	CANKRTR \cong NE-HE	10.64	2.82	156.18	63



GLU319 \cong OE1	AGNKRTR \cong NH2-HH22	23.45	2.78	161.11	157
GLU319 \cong OE2	AGNKRTR \cong NH1-HH12	20.88	2.82	159.17	87
GLU319 \cong OE2	AGNKRTR \cong NH2-HH22	17.49	2.79	160.57	107
GLU319 \cong OE1	AGNKRTR \cong NH1-HH12	16.88	2.83	157.88	170
AGNKRTR \cong O	TRP301 \cong NE1-HE1	16.07	2.84	157.22	46
PRO317 \cong O	AGNKRTR \cong NZ-HZ2	14.22	2.81	155.49	57
PRO317 \cong O	AGNKRTR \cong NZ-HZ1	13.77	2.81	154.35	47
ASP320 \cong OD1	AGNKRTR \cong NZ-HZ1	12.72	2.76	156.89	122
ASP320 \cong OD1	AGNKRTR \cong NZ-HZ3	12.47	2.77	156.77	114
ASP320 \cong OD2	AGNKRTR \cong NZ-HZ3	12.33	2.78	157.18	98
ASP320 \cong OD2	AGNKRTR \cong NZ-HZ1	11.92	2.77	157.47	169
PRO317 \cong O	AGNKRTR \cong NZ-HZ3	11.16	2.81	153.25	45
ASP320 \cong OD1	AGNKRTR \cong NZ-HZ2	10.53	2.77	156.41	65
ASP320 \cong OD2	AGNKRTR \cong NZ-HZ2	10.06	2.78	156.61	134

It is clear from Table 4 that Asp320 is the dominant amino acid for the interactions with the peptides. Figure 7 shows the profile of H-bonds created by Asp320 with the peptide ligands. This residue forms 3 consistent H-bonds with the CGNKRTR (tLyp-1, **1**). Consistent with the results presented in Table 4, only one of them is strong and present at high frequency while the two are relatively weak. All the mutated peptides **2-8** also interact with the Asp320 with at least one H-bond, but the H-bonds are relatively weaker compared to CGNKRTR (tLyp-1, **1**). The existence of mixed strong-moderate-weak H-bond pairings with the higher ratio of weak H-bonds might possibly be the reason for Asp320's reduced binding affinity to peptides due to interference with bulk water (see Table 5).^{68,69}

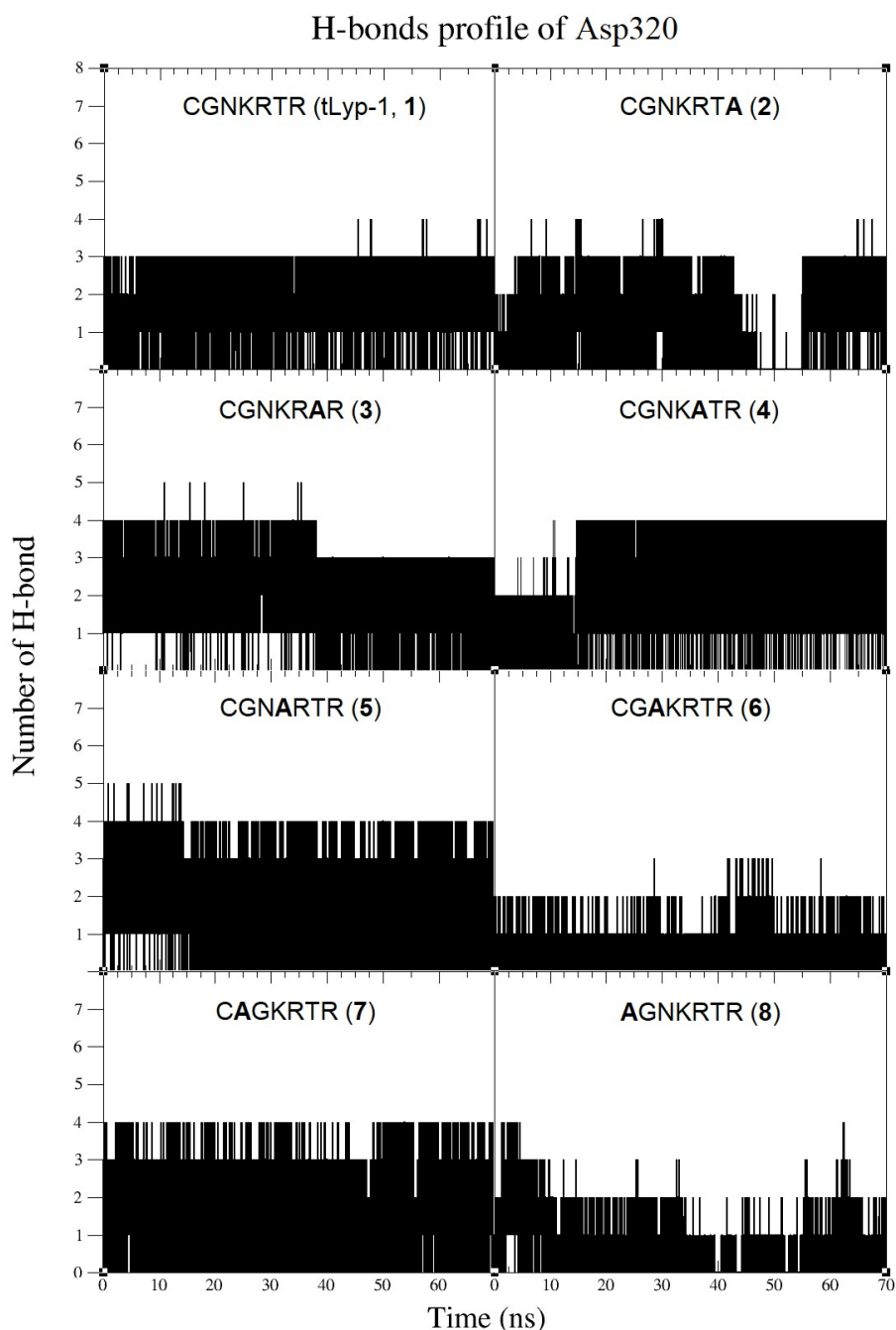


Figure 7. H-bond profile of the most dominant residue in the NRP-1 binding site (Asp320) with the tLyp-1 (CGNKRTR, **1**) and its mutated analogues (**2-8**) over the MD simulation time (0-70).

3.4.3. Binding Free Energy (MM-PBSA)

The binding free energy and its decompositional energies of the interactions between tLyp-1 (CGNKRTR, **1**) and its Ala-scan analogues (**2-8**) towards NRP-1 (Table 5) were calculated for the last 1 ns of the MD simulation time using the module of the Molecular Mechanics-Poisson Boltzmann surface area (MM-PBSA) programme in AMBER software with a neglected entropic contribution.^{32,33} The major contributions to this binding energy are the electrostatic, van der Waals as well as non-polar solvation terms.

Table 5 shows that tLyp-1 (CGNKRTR, **1**) and CGAKRTR (**6**) have the most favourable binding energies amongst all the peptides, with the $\Delta G_{bind}^* = -14.63 \pm 0.20$ kcal/mol and -14.26 ± 0.21 kcal/mol, respectively, followed by CANKRTR (**7**) (-12.96 ± 0.25 kcal/mol), CGNKRAR (**3**) (-9.84 ± 0.16 kcal/mol), AGNKRTR (**8**) (-8.33 ± 0.22 kcal/mol) and

CGNKATR (**4**) (-8.42 ± 0.18 kcal/mol). In general, binding of peptides is opposed by an unfavourable desolvation of polar groups, yielding a contribution in the range of 177.12 – 400.60 kcal/mol. Thus, although CANKRTR (**7**) has the most favourable intermolecular electrostatic interactions and second most favourable van der Waal interactions with NRP-1, its binding is over-compensated by the positive values of the desolvation term for the polar groups. This phenomenon is in fact, observed in the binding of all the peptides studied here and the reasons for this might be due to the interference with bulk water which could lead to increase in the electrostatic interactions with the water molecules thus increasing the polar solvation energy.^{68,69}

Table 5. Binding free energies (MM-PBSA) for CGNKRTR (tLyp-1, **1**) and its Ala-scan analogues (**2-8**) from MD simulation trajectories (69–70 ns).

Peptide No.	Peptide sequence	ΔG_{bind} kcal/mol	VDW kcal/mol	EEL kcal/mol	G_{polar} kcal/mol	$G_{non-polar}$ kcal/mol
1	CGNKRTR	-14.63 ± 0.20	-24.14 ± 0.11	-307.13 ± 0.81	341.42 ± 0.72	-24.78 ± 0.04
2	CGNKRTA	-3.60 ± 0.33	-33.06 ± 0.12	-120.11 ± 1.27	177.12 ± 1.33	-27.55 ± 0.07
3	CGNKRAR	-9.84 ± 0.16	-26.68 ± 0.11	-191.29 ± 0.59	232.46 ± 0.58	-24.32 ± 0.03
4	CGNKATR	-8.42 ± 0.18	-41.72 ± 0.11	-245.41 ± 0.72	310.86 ± 0.75	-32.14 ± 0.05
5	CGNARTR	10.96 ± 0.26	-33.18 ± 0.11	-264.54 ± 0.85	336.68 ± 0.75	-27.98 ± 0.04
6	CGAKRTR	-14.26 ± 0.21	-29.44 ± 0.12	-208.71 ± 1.23	250.42 ± 1.13	-26.53 ± 0.04
7	CANKRTR	-12.96 ± 0.25	-29.64 ± 0.13	-351.07 ± 0.76	400.60 ± 0.67	-32.84 ± 0.04
8	AGNKRTR	-8.83 ± 0.22	-19.79 ± 0.10	-273.08 ± 0.72	305.73 ± 0.70	-21.69 ± 0.04

ΔG_{bind} : binding free energy, **VDW**: van der Waals, **EEL**: electrostatic, G_{polar} : polar solvation energy, $G_{non-polar}$: non-polar solvation energy.

To reveal the critical amino acids of the NRP-1 binding site that participated in the binding with the peptide ligands, we calculated the MM-PBSA per residue decompositions of the most important residues in the NRP-1 binding site (i.e., Tyr297, Thr316, Asp320, Pro317, Thr349, and Tyr353) as shown in Figure 8. MM-PBSA per residue decompositions of the tLyp-1 (CGNKRTR, **1**) and its analogues (**2-8**) were also calculated (Figure 9).

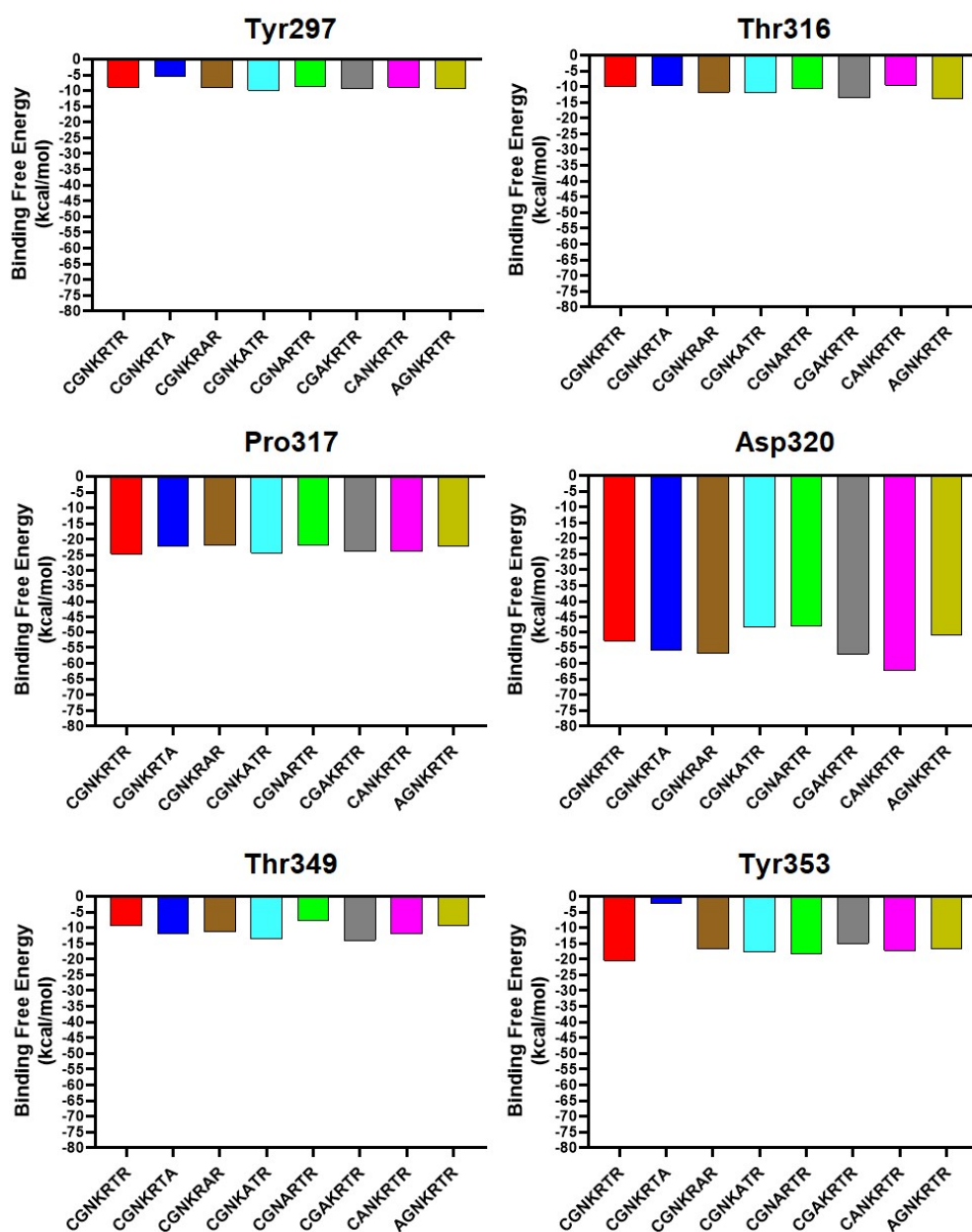


Figure 8. Contribution of the peptides with the key amino acids into the NRP-1 binding site using MM-PBSA per residue decomposition over the MD simulation time (69-70 ns).

In general, free binding energy values larger than 0 (positive energy) indicate that mutation is destabilizing the interaction, while negative energy indicates that mutation is stabilizing the interaction.⁷⁰ Asp320 appeared to be the most important residue that interact with the peptide ligands. Figure 8 shows that in general, all the peptide ligands made strong interactions with Asp320. tLyp-1 (CGNKRTR, **1**) interacted strongly with Asp320, Pro317 and Tyr353 (≈ -54 kcal/mol, ≈ -24 kcal/mol and ≈ -23 kcal/mol, respectively) compared to the other key residues. These interactions are contributed by the H-bond interactions between these three residues and the C-terminal Arg (Table 4 and Figure 9).

Replacing the C-terminal Arg with Ala (CGNKRTA, **2**) dramatically affects the affinity of the peptide. The free binding energy became less negative (-3.60 kcal/mol, Table 5). Furthermore, the MM-PBSA per residue for the peptide residue contribution (Figure 9) shows that the binding energy of the Ala residue is less negative (-50 kcal/mol) than the contribution of the Arg at the same position in the tLyp-1, indicating that the residue is affecting the

stabilization of the interaction with the NRP-1 binding site that results in the H-bond occupancy to lose to half (Table 4). Similarly, replacing Lys at position 4 (CGNARTR, **5**) also has a dominant influence on the affinity towards NRP-1 as predicted from ΔG_{bind}^* , from -14.63 ± 0.20 kcal/mol by the native peptide to 10.96 ± 0.26 kcal/mol by the peptide analogue. In addition, the H-bond occupancy (Table 4) shows that the CGNARTR (**5**) formed H-bonds with very low frequency compared to tLyp-1 (CGNKRTR, **1**). This, reflects the importance of Arg and Lys at these positions, as confirmed by the binding affinity results (IC_{50} for **2** was not determined (i.e., beyond the micromolar concentration) and for **5** is $50 \mu\text{M}$). These values are very high compared to the wild-type peptide, t-Lyp-1 (**1**, $4 \mu\text{M}$) showing marked decrease in activity in these analogues. All these results thus confirm the importance of CendR motif in peptides targeting NRP-1.

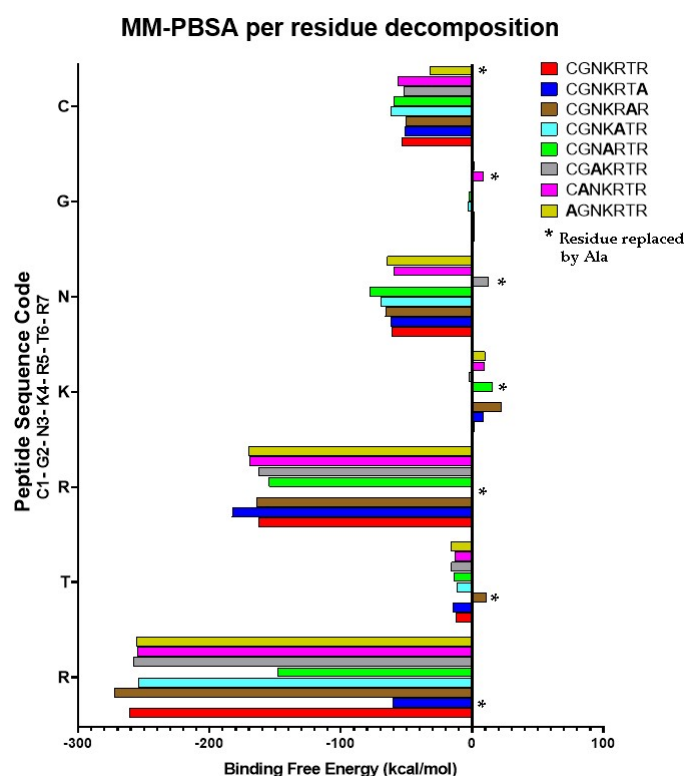


Figure 9. Contribution of the critical peptide residues into the binding site using MM-PBSA per residue decomposition over the MD simulation time (69-70 ns).

Mutation at positions 1 (AGNKRTR, **8**), 2 (CANKRTR, **7**), 3 (CGAKRTR, **6**), 5 (CGNKATR, **4**), and 6 (CGNKRAR, **3**) did not significantly affect the binding as the corresponding Ala-scan analogues can still bind to NRP-1 binding site, albeit with lower ΔG_{bind}^* . Contrary to the experimental binding affinity results, changing Cys and Gly at the N-terminal and position 2 do have some effects on the binding of the peptides in the b1 binding site of NRP-1. However, it is obvious that these peptides (CANKRTR (**7**) and AGNKRTR (**8**)) formed favourable interactions with the most important residue in the NRP-1 binding site (Asp320), as shown in Figure 8, and both analogues were found to interact with the other key amino acids into the binding site, albeit with low frequency (Table 4). It should be noted that the MM-PBSA per residue decomposition analysis was carried out with neglected entropy contributions to the binding free energies due to the high molecular weight of the wild-type and its mutated species. Therefore, the calculated energies might not significantly affect the outcome of the overall binding free energy.^{14,71,72} However, many aspects must be considered

in future work, such as investigating the possibility of tLyp-1 and its Ala-scan analogues interacting with the all NRP-1 domains.

4. Conclusion

In this paper, we reported the molecular docking, the synthesis and *in vitro* binding affinity tests, and the MD simulation study on the interaction between tLyp-1 and its Ala-scan analogues on the NRP-1 receptor. The finding supports the CendR motif, in which the most important amino acids are the C-terminal Arg and Lys-4 in the CGNKRTR (tLyp-1) sequence. Replacing the C-terminal Arg was proven to be detrimental to the binding affinity of tLyp-1 on NRP-1. The importance of Lys at position 4 was confirmed by the MM-PBSA analysis and this was further reiterated with the *in vitro* LBA that showed an increment in the IC₅₀ value from 4 μM for the native peptide (CGNKRTR, tLyp-1) into 50 μM for the CGNARTR analogue, following substitution of Lys-4 with Ala in the sequence. Furthermore, the fact that Cys is inessential could be useful for future synthesis. As the fixation of this last amino acid to the peptide was found to be challenging, substituting this amino acid with another may be a good option to improve the efficiency of the peptide synthesis. The finding in this study will serve as a guide in the future development of tLyp-1 as a targeting agent towards NRP-1 receptor. The peptide may be modified and coupled with suitable molecules to be delivered to the NRP-1 expressed cells, that will be useful in the detection and treatment of cancer *via* the angiogenesis pathway.

Acknowledgments

This work was supported by the “Ministère de l’Enseignement Supérieur, de la Recherche et de l’Innovation” (MSERI) with a Doctoral fellowship for Ludivine Larue.

Disclosure statement

The authors declare no conflict of interest.

References

1. Ryerson, A.B.; Ehemann, C.R.; Altekruse, S.F.; Ward, J.W.; Jemal, A.; Sherman, R.L.; Henley, S.J.; Holtzman, D.; Lake, A.; Noone, A.M. Annual Report to the Nation on the Status of Cancer, 1975-2012, featuring the increasing incidence of liver cancer. *Cancer* **2016**, *122*, 1312-1337. DOI: [10.1002/cncr.29936](https://doi.org/10.1002/cncr.29936)
2. Liu, M.; Fang, X.; Yang, Y.; Wang, C. Peptide-enabled targeted delivery systems for therapeutic applications. *Frontiers in Bioengineering and Biotechnology* 2021, *9*, 701504. DOI: [10.3389/fbioe.2021.701504](https://doi.org/10.3389/fbioe.2021.701504)
3. Tirand, L.; Frochot, C.; Vanderesse, R.; Thomas, N.; Trinquet, E.; Pinel, S.; Viriot, M.-L.; Guillemin, F.; Barberi-Heyob, M. A peptide competing with VEGF165 binding on neuropilin-1 mediates targeting of a chlorin-type photosensitizer and potentiates its photodynamic activity in human endothelial cells. *Journal of Controlled Release* **2006**, *111*, 153-164. DOI: [10.1016/j.jconrel.2005.11.017](https://doi.org/10.1016/j.jconrel.2005.11.017)
4. Couleaud, P.; Morosini, V.; Frochot, C.; Richeter, S.; Raehm, L.; Durand, J.-O. Silica-based nanoparticles for photodynamic therapy applications. *Nanoscale* **2010**, *2*, 1083-1095. DOI: [10.1039/c0nr00096e](https://doi.org/10.1039/c0nr00096e)
5. Thomas, E.; Colombeau, L.; Gries, M.; Peterlini, T.; Mathieu, C.; Thomas, N.; Boura, C.; Frochot, C.; Vanderesse, R.; Lux, F. Ultrasmall AGuIX theranostic nanoparticles for vascular-targeted interstitial photodynamic therapy of glioblastoma. *International Journal of Nanomedicine* **2017**, *12*, 7075-7088. DOI: [10.2147/IJN.S141559](https://doi.org/10.2147/IJN.S141559)
6. Youssef, Z.; Yesmurzayeva, N.; Larue, L.; Jouan-Hureaux, V.; Colombeau, L.; Arnoux, P.; Acherar, S.; Vanderesse, R.; Frochot, C. New Targeted Gold Nanorods for the Treatment of Glioblastoma by Photodynamic Therapy. *Journal of Clinical Medicine* **2019**, *8*, 2205. DOI: [10.3390/jcm8122205](https://doi.org/10.3390/jcm8122205)

7. Gries, M.; Thomas, N.; Daouk, J.; Rocchi, P.; Choulier, L.; Jubréaux, J.; Pierson, J.; Reinhard, A.; Jouan-Hureau, V.; Château, A.; Acherar, S.; Frochot, C.; Lux, F.; Tillement, O.; Barberi-Heyob, M. Multiscale selectivity and in vivo biodistribution of NRP-1-targeted theranostic AGuIX nanoparticles for PDT of glioblastoma. *International Journal of Nanomedicine* **2020**, *15*, 8739-8758. DOI: [10.2147/IJN.S261352](https://doi.org/10.2147/IJN.S261352)
8. Larue, L.; Moussounda Koumba, T.; Le Breton, N.; Vilen, B.; Arnoux, P.; Jouan-Hureau, V.; Boura, C.; Audran, G.; Bikanga, R.; Marque, S. R. A., Acherar, S.; Frochot, C. Design of a targeting and oxygen-independent platform to improve photodynamic therapy: A proof of concept. *ACS Applied Bio Materials* **2021**, *4*, 1330-1339. DOI: [10.1021/acsabm.0c01227](https://doi.org/10.1021/acsabm.0c01227)
9. Moussaron, A.; Jouan-Hureau, V.; Collet, C.; Pierson, J.; Thomas, N.; Choulier, L.; Veran, N.; Doyen, M.; Arnoux, P.; Maskali, F.; Dumas, D.; Acherar, S.; Barberi-Heyob, M.; Frochot, C. Preliminary study of new gallium-68 radiolabeled peptide targeting NRP-1 to detect brain metastases by positron emission tomography. *Molecules* **2021**, *26*, 7273. DOI: [10.3390/molecules26237273](https://doi.org/10.3390/molecules26237273)
10. Laakkonen, P.; Porkka, K.; Hoffman, J.A.; Ruoslahti, E. A tumor-homing peptide with a targeting specificity related to lymphatic vessels. *Nature Medicine* **2002**, *8*, 751-755. DOI: [10.1038/nm720](https://doi.org/10.1038/nm720)
11. Enbäck, J.; Laakkonen, P. Tumour-homing peptides: tools for targeting, imaging and destruction. *Biochemical Society Transactions* **2007**, *35*, 780-783. DOI: [10.1042/BST0350780](https://doi.org/10.1042/BST0350780)
12. Ciobanasi, C.; Dragomir, I.; Apetrei, A. The penetrating properties of the tumor homing peptide LyP-1 in model lipid membranes. *Journal of Peptide Science* **2019**, *25*, e3145. DOI: [10.1002/psc.3145](https://doi.org/10.1002/psc.3145)
13. Wu, H.-b.; Wang, Z.; Wang, Q.-s.; Han, Y.-j.; Wang, M.; Zhou, W.-l.; Li, H.-s. Use of labelled tLyP-1 as a novel ligand targeting the NRP receptor to image glioma. *PLoS One* **2015**, *10*, e0137676. DOI: [10.1371/journal.pone.0137676](https://doi.org/10.1371/journal.pone.0137676)
14. Timur, S.S.; Yalçın, G.; Çevik, Ö.; Andaç, C.; Gürsoy, R.N. Molecular dynamics, thermodynamic, and mutational binding studies for tumor-specific LyP-1 in complex with p32. *Journal of Biomolecular Structure and Dynamics* **2018**, *36*, 1134-1144. DOI: [10.1080/07391102.2017.1313779](https://doi.org/10.1080/07391102.2017.1313779)
15. Kamarulzaman, E.E.; Gazzali, A.M.; Acherar, S.; Frochot, C.; Barberi-Heyob, M.; Boura, C.; Chaimbault, P.; Sibille, E.; Wahab, H.A.; Vanderesse, R. New peptide-conjugated chlorin-type photosensitizer targeting neuropilin-1 for anti-vascular targeted photodynamic therapy. *International Journal of Molecular Sciences* **2015**, *16*, 24059-24080. DOI: [10.3390/ijms161024059](https://doi.org/10.3390/ijms161024059)
16. Berman, H.; Henrick, K.; Nakamura, H. Announcing the worldwide protein data bank. *Nature Structural & Molecular Biology* **2003**, *10*, 980-980. DOI: [10.1038/nsb1203-980](https://doi.org/10.1038/nsb1203-980)
17. Eldrid, C.; Yu, L.; Yelland, T.; Fotinou, C.; Djordjevic, S. Neuropilin 1-b1 domain in a complex with the C-terminal VEGFB186 peptide. **2020**, 10.2210/pdb6TKK/pdb. PDB DOI: [10.2210/pdb6TKK/pdb](https://doi.org/10.2210/pdb6TKK/pdb)
18. Biovia, D.S. Discovery studio visualizer. **2017**, Vol 936.; *Biovia: San Diego, CA, USA, 2017*.
19. Dolinsky, T.J.; Czodrowski, P.; Li, H.; Nielsen, J.E.; Jensen, J.H.; Klebe, G.; Baker, N.A. PDB2PQR: expanding and upgrading automated preparation of biomolecular structures for molecular simulations. *Nucleic Acids Research* **2007**, *35*, W522-W525. DOI: [10.1093/nar/gkm276](https://doi.org/10.1093/nar/gkm276)
20. Olsson, M.H.; Søndergaard, C.R.; Rostkowski, M.; Jensen, J.H. PROPKA3: consistent treatment of internal and surface residues in empirical p K a predictions. *Journal of Chemical Theory and Computation* **2011**, *7*, 525-537. DOI: [10.1021/ct100578](https://doi.org/10.1021/ct100578)
21. Al-Thiabat, M.G.; Gazzali, A.M.; Mohtar, N.; Murugaiyah, V.; Kamarulzaman, E.E.; Yap, B.K.; Rahman, N.A.; Othman, R.; Wahab, H.A. Conjugated β -Cyclodextrin Enhances the Affinity of Folic Acid towards FR α : Molecular Dynamics Study. *Molecules* **2021**, *26*, 5304. DOI: [10.3390/molecules26175304](https://doi.org/10.3390/molecules26175304)
22. Williams, C.J.; Headd, J.J.; Moriarty, N.W.; Prisant, M.G.; Videau, L.L.; Deis, L.N.; Verma, V.; Keedy, D.A.; Hintze, B.J.; Chen, V.B. MolProbity: More and better reference data for

- improved all-atom structure validation. *Protein Science* **2018**, *27*, 293-315. DOI: [10.1002/pro.3330](https://doi.org/10.1002/pro.3330)
23. Pettersen, E.F.; Goddard, T.D.; Huang, C.C.; Couch, G.S.; Greenblatt, D.M.; Meng, E.C.; Ferrin, T.E. UCSF Chimera—a visualization system for exploratory research and analysis. *Journal of Computational Chemistry* **2004**, *25*, 1605-1612. DOI: [10.1002/jcc.20084](https://doi.org/10.1002/jcc.20084)
 24. Kamarulzaman, E.E.; Vanderesse, R.; Gazzali, A.M.; Barberi-Heyob, M.; Boura, C.; Frochot, C.; Shawkataly, O.; Aubry, A.; Wahab, H.A. Molecular modelling, synthesis and biological evaluation of peptide inhibitors as anti-angiogenic agent targeting neuropilin-1 for anticancer application. *Journal of Biomolecular Structure and Dynamics* **2017**, *35*, 26-45. DOI: [10.1080/07391102.2015.1131196](https://doi.org/10.1080/07391102.2015.1131196)
 25. Morris, G.M.; Huey, R.; Lindstrom, W.; Sanner, M.F.; Belew, R.K.; Goodsell, D.S.; Olson, A.J. AutoDock4 and AutoDockTools4: Automated docking with selective receptor flexibility. *Journal of Computational Chemistry* **2009**, *30*, 2785-2791. DOI: [10.1002/jcc.21256](https://doi.org/10.1002/jcc.21256)
 26. Zhang, Y.; Sanner, M.F. AutoDock CrankPep: combining foldingF and docking to predict protein-peptide complexes. *Bioinformatics* **2019**, *35*, 5121-5127. DOI: [10.1093/bioinformatics/btz459](https://doi.org/10.1093/bioinformatics/btz459)
 27. Schrodinger, L. The PyMOL molecular graphics system. *Version* **2010**, *1*, 0.
 28. Xiong, G.; Wu, Z.; Yi, J.; Fu, L.; Yang, Z.; Hsieh, C.; Yin, M.; Zeng, X.; Wu, C.; Lu, A.; Chen, X.; Hou, T.; Cao, D. ADMETlab 2.0: an integrated online platform for accurate and comprehensive predictions of ADMET properties. *Nucleic Acids Research* **2021**, *49*, W5-W14. DOI: [10.1093/nar/gkab255](https://doi.org/10.1093/nar/gkab255)
 29. Case, D.; Ben-Shalom, I.; Brozell, S.; Cerutti, D.; Cheatham III, T.; Cruzeiro, V.; Darden, T.; Duke, R.; Ghoreishi, D.; Gilson, M. AMBER 2018: San Francisco. California: 2018.
 30. Al-Thiabat, M.G.; Saqallah, F.G.; Gazzali, A.M.; Mohtar, N.; Yap, B.K.; Choong, Y.S.; Wahab, H.A. Heterocyclic Substitutions Greatly Improve Affinity and Stability of Folic Acid towards FR α . an In Silico Insight. *Molecules* **2021**, *26*, 1079. DOI: [10.3390/molecules26041079](https://doi.org/10.3390/molecules26041079)
 31. Andersen, H.C. Rattle: A “velocity” version of the shake algorithm for molecular dynamics calculations. *Journal of Computational Physics* **1983**, *52*, 24-34. DOI: [10.1016/0021-9991\(83\)90014-1](https://doi.org/10.1016/0021-9991(83)90014-1)
 32. Tan, C.; Tan, Y.-H.; Luo, R. Implicit nonpolar solvent models. *The Journal of Physical Chemistry B* **2007**, *111*, 12263-12274. DOI: [10.1021/jp073399n](https://doi.org/10.1021/jp073399n)
 33. Miller III, B.R.; McGee Jr, T.D.; Swails, J.M.; Homeyer, N.; Gohlke, H.; Roitberg, A.E. MMPBSA.py: an efficient program for end-state free energy calculations. *Journal of Chemical Theory and Computation*. **2012**, *8*, 3314-3321. DOI: [10.1021/ct300418h](https://doi.org/10.1021/ct300418h)
 34. Powell, J.; Mota, F.; Steadman, D.; Soudy, C.; Miyauchi, J.T.; Crosby, S.; Jarvis, A.; Reisinger, T.; Winfield, N.; Evans, G. Small molecule neuropilin-1 antagonists combine antiangiogenic and antitumor activity with immune modulation through reduction of transforming growth factor beta (TGF β) production in regulatory T-cells. *Journal of Medicinal Chemistry* **2018**, *61*, 4135-4154. DOI: [10.1021/acs.jmedchem.8b00210](https://doi.org/10.1021/acs.jmedchem.8b00210)
 35. Mota, F.; Fotinou, C.; Rana, R.R.; Chan, A.E.; Yelland, T.; Arooz, M.T.; O'Leary, A.P.; Hutton, J.; Frankel, P.; Zachary, I. Architecture and hydration of the arginine-binding site of neuropilin-1. *The FEBS Journal* **2018**, *285*, 1290-1304. DOI: [10.1111/febs.14405](https://doi.org/10.1111/febs.14405)
 36. Didierjean, C., Jelsch, C. Crystal Structure of the b1 Domain of Human Neuropilin-1 in complex with a bicine molecule. **2016**, 10.2210/pdb5C7G/pdb. PDB DOI: [10.2210/pdb5C7G/pdb](https://doi.org/10.2210/pdb5C7G/pdb)
 37. Allerston, C.K., Yelland, T.S., Jarvis, A., Jenkins, K., Winfield, N., Cheng, L., Jia, H., Zachary, I., Selwood, D.L., Djordjevic, S. B1 domain of human Neuropilin-1 with acetate ion in a ligand-binding site. **2015**, 10.2210/pdb4RN5/pdb. PDB DOI: [10.2210/pdb4RN5/pdb](https://doi.org/10.2210/pdb4RN5/pdb)
 38. Appleton, B.A.; Wu, P.; Maloney, J.; Yin, J.; Liang, W.C.; Stawicki, S.; Mortara, K.; Bowman, K.K.; Elliott, J.M.; Desmarais, W. Structural studies of neuropilin/antibody complexes provide insights into semaphorin and VEGF binding. *The EMBO Journal* **2007**, *26*, 4902-4912. DOI: [10.1038/sj.emboj.7601906](https://doi.org/10.1038/sj.emboj.7601906)
 39. Lee, C.C.; Kreuzsch, A.; McMullan, D.; Ng, K.; Spraggon, G. Crystal structure of the human neuropilin-1 b1 domain. *Structure* **2003**, *11*, 99-108. DOI: [10.1016/s0969-2126\(02\)00941-3](https://doi.org/10.1016/s0969-2126(02)00941-3)
 40. Tsai, Y.C.I.; Fotinou, C.; Rana, R.; Yelland, T.; Frankel, P.; Zachary, I.; Djordjevic, S. Structural studies of neuropilin-2 reveal a zinc ion binding site remote from the vascular

- endothelial growth factor binding pocket. *The FEBS Journal* **2016**, *283*, 1921-1934. DOI: [10.1111/febs.13711](https://doi.org/10.1111/febs.13711)
41. Yelland, T.; Djordjevic, S. Crystal structure of the neuropilin-1 MAM domain: completing the neuropilin-1 ectodomain picture. *Structure* **2016**, *24*, 2008-2015. DOI: [10.1016/j.str.2016.08.017](https://doi.org/10.1016/j.str.2016.08.017)
 42. Daly, J.L.; Simonetti, B.; Klein, K.; Chen, K.-E.; Williamson, M.K.; Antón-Plágaro, C.; Shoemark, D.K.; Simón-Gracia, L.; Bauer, M.; Hollandi, R. Neuropilin-1 is a host factor for SARS-CoV-2 infection. *Science* **2020**, *370*, 861-865. DOI: [10.1126/science.abd3072](https://doi.org/10.1126/science.abd3072)
 43. Parker, M.W.; Xu, P.; Li, X.; Vander Kooi, C.W. Structural basis for selective vascular endothelial growth factor-A (VEGF-A) binding to neuropilin-1. *Journal of Biological Chemistry* **2012**, *287*, 11082-11089. DOI: [10.1074/jbc.M111.331140](https://doi.org/10.1074/jbc.M111.331140)
 44. Jarvis, A.; Allerston, C.K.; Jia, H.; Herzog, B.; Garza-Garcia, A.; Winfield, N.; Ellard, K.; Aqil, R.; Lynch, R.; Chapman, C. Small molecule inhibitors of the neuropilin-1 vascular endothelial growth factor A (VEGF-A) interaction. *Journal of Medicinal Chemistry* **2010**, *53*, 2215-2226. DOI: [10.1021/jm901755g](https://doi.org/10.1021/jm901755g)
 45. Vander Kooi, C.W.; Jusino, M.A.; Perman, B.; Neau, D.B.; Bellamy, H.D.; Leahy, D.J. Structural basis for ligand and heparin binding to neuropilin B domains. *Proceedings of the National Academy of Sciences* **2007**, *104*, 6152-6157. DOI: [10.1073/pnas.0700043104](https://doi.org/10.1073/pnas.0700043104)
 46. Janssen, B.J.; Malinauskas, T.; Weir, G.A.; Cader, M.Z.; Siebold, C.; Jones, E.Y. Neuropilins lock secreted semaphorins onto plexins in a ternary signaling complex. *Nature Structural & Molecular Biology* **2012**, *19*, 1293-1299. DOI: [10.1038/nsmb.2416](https://doi.org/10.1038/nsmb.2416)
 47. Huey, R.; Morris, G.M.; Forli, S. Using AutoDock 4 and AutoDock vina with AutoDockTools: a tutorial. *The Scripps Research Institute Molecular Graphics Laboratory* **2012**, *10550*, 92037. [link](#)
 48. Jacob, R.B.; Bullock, C.W.; Andersen, T.; McDougal, O.M. DockoMatic: Automated peptide analog creation for high throughput virtual screening. *Journal of Computational Chemistry* **2011**, *32*, 2936-2941. DOI: [10.1002/jcc.21864](https://doi.org/10.1002/jcc.21864)
 49. Rentzsch, R.; Renard, B.Y. Docking small peptides remains a great challenge: an assessment using AutoDock Vina. *Briefings in Bioinformatics* **2015**, *16*, 1045-1056. DOI: [10.1093/bib/bbv008](https://doi.org/10.1093/bib/bbv008)
 50. Puszko, A.K.; Sosnowski, P.; Raynaud, F.; Hermine, O.; Hopfgartner, G.; Lepelletier, Y.; Misicka, A. Does Cysteine Rule (CysR) Complete the CendR Principle? Increase in Affinity of Peptide Ligands for NRP-1 Through the Presence of N-Terminal Cysteine. *Biomolecules* **2020**, *10*, 448. DOI: [10.3390/biom10030448](https://doi.org/10.3390/biom10030448)
 51. Hicklin, D.J.; Ellis, L.M. Role of the vascular endothelial growth factor pathway in tumor growth and angiogenesis. *Journal of Clinical Oncology* **2005**, *23*, 1011-1027. DOI: [10.1200/JCO.2005.06.081](https://doi.org/10.1200/JCO.2005.06.081)
 52. Teesalu, T.; Sugahara, K.N.; Kotamraju, V.R.; Ruoslahti, E. C-end rule peptides mediate neuropilin-1-dependent cell, vascular, and tissue penetration. *Proceedings of the National Academy of Sciences* **2009**, *106*, 16157-16162. DOI: [10.1073/pnas.0908201106](https://doi.org/10.1073/pnas.0908201106)
 53. Fedorczyk, B.; Lipiński, P.F.; Puszko, A.K.; Tymecka, D.; Wilenska, B.; Dudka, W.; Perret, G.Y.; Wiczorek, R.; Misicka, A. Triazolepeptides inhibiting the interaction between neuropilin-1 and vascular endothelial growth factor-165. *Molecules* **2019**, *24*, 1756. DOI: [10.3390/molecules24091756](https://doi.org/10.3390/molecules24091756)
 54. van de Waterbeemd, H.; Gifford, E. ADMET in silico modelling: towards prediction paradise? *Nature Reviews Drug Discovery* **2003**, *2*, 192-204. DOI: [10.1038/nrd1032](https://doi.org/10.1038/nrd1032)
 55. Di, L.; Kerns, E. Drug-like properties concepts, structure design and methods from ADME to toxicity optimization (2nd edition, Academic Press: Boston, MA, USA, 2016). DOI: [10.1016/C2013-0-18378-X](https://doi.org/10.1016/C2013-0-18378-X)
 56. Vrbanac, J.; Slauter, R. Chapter 3—Blood-brain barrier, pp 39-67. In Faqi, A. S. ed *A comprehensive guide to toxicology in nonclinical drug development* (2nd edition, Academic Press: London, UK, 2017). DOI: [10.1016/B978-0-12-803620-4.00003-7](https://doi.org/10.1016/B978-0-12-803620-4.00003-7)
 57. Wang, N.-N.; Dong, J.; Deng, Y.-H.; Zhu, M.-F.; Wen, M.; Yao, Z.-J.; Lu, A.-P.; Wang, J.-B.; Cao, D.-S. ADME properties evaluation in drug discovery: prediction of Caco-2 cell

- permeability using a combination of NSGA-II and boosting. *Journal of Chemical Information and Modeling* **2016**, *56*, 763-773. DOI: [10.1021/acs.jcim.5b00642](https://doi.org/10.1021/acs.jcim.5b00642)
58. Wang, N.-N.; Huang, C.; Dong, J.; Yao, Z.-J.; Zhu, M.-F.; Deng, Z.-K.; Lv, B.; Lu, A.-P.; Chen, A. F.; Cao, D.-S. Predicting human intestinal absorption with modified random forest approach: a comprehensive evaluation of molecular representation, unbalanced data, and applicability domain issues. *RSC Advances* **2017**, *7*, 19007-19018. DOI: [10.1039/C6RA28442F](https://doi.org/10.1039/C6RA28442F)
59. Ika, M.; Sharma, A.; Aggarwal, V.; Sharma, M.; Dhingra, N. Lantadenes Targeting NF-KB in Cancer: Molecular Docking and ADMET Predictions. *International Journal of Life science and Pharma Research* **2021**, *11*, P114-P122. DOI: [10.22376/ijpbs/lpr.2021.11.2.P114-122](https://doi.org/10.22376/ijpbs/lpr.2021.11.2.P114-122)
60. Clark, D. E. In silico prediction of blood–brain barrier permeation. *Drug Discovery Today* **2003**, *8*, 927-933. DOI: [10.1016/S1359-6446\(03\)02827-7](https://doi.org/10.1016/S1359-6446(03)02827-7)
61. Kazmi, S. K.; Jun, R.; Yu, M.-S.; Jung, C.; Na, D. In silico approaches and tools for the prediction of drug metabolism and fate: A review. *Computers in Biology and Medicine* **2019**, *106*, 54-64. DOI: [10.1016/j.combiomed.2019.01.008](https://doi.org/10.1016/j.combiomed.2019.01.008)
62. Yang, H.; Sun, L.; Li, W.; Liu, G. ; Tang, Y. In silico prediction of chemical toxicity for drug design using machine learning methods and structural alerts. *Frontiers in Chemistry* **2018**, *6*, 30. DOI: [10.3389/fchem.2018.00030](https://doi.org/10.3389/fchem.2018.00030)
63. von Wronski, M.A.; Raju, N.; Pillai, R.; Bogdan, N.J.; Marinelli, E.R.; Nanjappan, P.; Ramalingam, K.; Arunachalam, T.; Eaton, S.; Linder, K.E. Tuftsin binds neuropilin-1 through a sequence similar to that encoded by exon 8 of vascular endothelial growth factor. *Journal of Biological Chemistry* **2006**, *281*, 5702-5710. DOI: [10.1074/jbc.M511941200](https://doi.org/10.1074/jbc.M511941200)
64. Wells, J.A.; McClendon, C.L. Reaching for high-hanging fruit in drug discovery at protein–protein interfaces. *Nature* **2007**, *450*, 1001-1009. DOI: [10.1038/nature06526](https://doi.org/10.1038/nature06526)
65. Ivanov, A.A.; Khuri, F.R.; Fu, H. Targeting protein–protein interactions as an anticancer strategy. *Trends in Pharmacological Sciences* **2013**, *34*, 393-400. DOI: [10.1016/j.tips.2013.04.007](https://doi.org/10.1016/j.tips.2013.04.007)
66. Le, T.H.V.; Kwon, S.-M. Vascular Endothelial Growth Factor Biology and Its Potential as a Therapeutic Target in Rheumatic Diseases. *International Journal of Molecular Sciences* **2021**, *22*, 5387. DOI: [10.3390/ijms22105387](https://doi.org/10.3390/ijms22105387)
67. Ruoslahti, E. Tumor penetrating peptides for improved drug delivery. *Advanced Drug Delivery Reviews* **2017**, *110*, 3-12. DOI: [10.1016/j.addr.2016.03.008](https://doi.org/10.1016/j.addr.2016.03.008)
68. Lafont, V.; Armstrong, A.A.; Ohtaka, H.; Kiso, Y.; Mario Amzel, L.; Freire, E. Compensating enthalpic and entropic changes hinder binding affinity optimization. *Chemical Biology & Drug Design* **2007**, *69*, 413-422. DOI: [10.1111/j.1747-0285.2007.00519.x](https://doi.org/10.1111/j.1747-0285.2007.00519.x)
69. Chen, D.; Oezguen, N.; Urvil, P.; Ferguson, C.; Dann, S.M.; Savidge, T.C. Regulation of protein-ligand binding affinity by hydrogen bond pairing. *Science Advances* **2016**, *2*, e1501240. DOI: [10.1126/sciadv.1501240](https://doi.org/10.1126/sciadv.1501240)
70. Şeref, G. In silico drug repositioning against human NRP1 to block SARS-CoV-2 host entry. *Turkish Journal of Biology* **2021**, *45*, 442-458. DOI: [10.3906/biy-2012-52](https://doi.org/10.3906/biy-2012-52)
71. Sun, H.; Duan, L.; Chen, F.; Liu, H.; Wang, Z.; Pan, P.; Zhu, F.; Zhang, J.Z.; Hou, T. Assessing the performance of MM/PBSA and MM/GBSA methods. 7. Entropy effects on the performance of end-point binding free energy calculation approaches. *Physical Chemistry Chemical Physics* **2018**, *20*, 14450-14460. DOI: [10.1039/c7cp07623a](https://doi.org/10.1039/c7cp07623a)
72. Hou, T.; Wang, J.; Li, Y.; Wang, W. Assessing the performance of the MM/PBSA and MM/GBSA methods. 1. The accuracy of binding free energy calculations based on molecular dynamics simulations. *Journal of Chemical Information and Modeling* **2011**, *51*, 69-82. DOI: [10.1021/ci100275a](https://doi.org/10.1021/ci100275a)